JOURNAL OF GEOPHYSICAL RESEARCH, VOL. 106, NO. D10, PAGES 10,257–10,274, MAY 27, 2001

Empirical age spectra for the midlatitude lower stratosphere from in situ observations of CO_2: Quantitative evidence for a subtropical "barrier" to horizontal transport

A. E. Andrews,[1,2] K. A. Boering,[3] S. C. Wofsy,[1] B. C. Daube,[1] D. B. Jones,[1]
S. Alex,[1] M. Loewenstein,[4] J. R. Podolske,[4] and S. E. Strahan[5]

Abstract. Empirical age spectra for the northern midlatitude lower stratosphere were derived using a genetic algorithm constrained by in situ observations of CO_2 and N_2O. An age spectrum is the probability distribution function describing the ensemble of transit times between the tropical tropopause and a point in the stratosphere. Age spectra with two distinct maxima fit observed CO_2 mixing ratios significantly better than age spectra consisting of a single peak. The mean transit time (mean age) of the younger peak increased with altitude from the tropopause to ~1 year at 19.5 km, while the mean age of the older peak was 5.4 ± 0.4 years throughout this altitude region. Near the tropopause, ~10% of the air was represented by the older peak, increasing to ~50% at 19.5 km. We argue that the younger peak represents rapid quasihorizontal transport of air from the tropics, while the older peak represents downwelling of air from higher altitudes in the mean meridional circulation. Mean ages for the younger and older peaks provide estimates of the residence times for air in the lower and middle stratosphere, respectively. The clear separation of the peaks implies a significant altitude region where there is little meridional exchange between midlatitudes and the tropics.

1. Introduction

Deficiencies in our knowledge of stratospheric transport rates and the underlying dynamical processes are major factors limiting efforts to model stratospheric ozone and to predict changes in stratospheric composition due to perturbations such as climate change, accumulation of greenhouse gases, volcanic eruptions, growth and decay of industrial halocarbons, or exhaust from a possible future fleet of stratospheric aircraft. It is generally agreed that air enters the stratosphere mainly at the tropical tropopause and is then transported to higher altitudes and latitudes by the combined effects of the mean meridional ("Brewer-Dobson") circulation and eddy transport [e.g., *Holton et al.*, 1995]. However, quantitative information about stratospheric transport rates is difficult to derive, and many aspects of the circulation remain poorly understood.

For example, a recent objective of the atmospheric science community has been to determine the impact of gas phase and particulate emissions that would be injected into the midlatitude lower stratosphere by supersonic aircraft. One of the primary sources of uncertainty in impact assessment studies is how much of the exhaust would be transported into the lower tropical stratosphere, where it could be lofted into the ozone production region, versus how much would simply be flushed into the troposphere [*Kawa et al.*, 1999]. More generally, export of young air from the tropics to midlatitudes and recirculation of photochemically aged air back into the tropics have a significant impact on the residence time of pollutants in the stratosphere. Thus developing the ability to confidently predict the stratospheric response to natural or anthropogenic perturbations will require accurate knowledge of transport rates among and within the troposphere and the tropical and extratropical stratosphere.

To this end, much effort has been devoted to defining and refining conceptual models that describe observed tracer distributions and relationships among tracers. *Plumb and Ko* [1992] sought to explain observations during the 1980s of compact correlations among mixing ratios of long-lived trace species and showed that compact relationships among tracers exist when the timescales for horizontal transport are much faster than the local photochemical lifetime. That study implicitly assumed that, on an annually averaged basis, isentropic mixing operates on a global scale (i.e., from pole to pole), and the paradigm they described has come to be known as the "global diffuser model". The "tropical pipe model" [*Plumb*, 1996] was proposed to explain aerosol and tracer data which indicate that mixing of air between the tropics and higher latitudes is inhibited [e.g., *Goldan et al.*, 1980; *Murphy et al.*, 1993; *Randel et al.*, 1993]. It is a variation of the Plumb and Ko framework, in which quasihorizontal mixing by breaking planetary waves occurs rapidly at midlatitudes but is diminished in the tropics. Accumulating evidence suggests that some exchange between the tropical and extratropi-

[1]Department of Earth and Planetary Sciences and the Division of Engineering and Applied Sciences, Harvard University, Cambridge, Massachusetts
[2]Now at NASA Goddard Space Flight Center, Greenbelt, Maryland.
[3]Departments of Chemistry and of Earth and Planetary Science, University of California, Berkeley, California
[4]NASA Ames Research Center, Moffett Field, California.
[5]General Sciences Corporation, Beltsville, Maryland

Paper number 2000JD900703.
0148-0277/01/2000JD900703$09.00

cal stratosphere does occur at some altitudes [e.g., *Feely and Spar*, 1960; *Telegadas and List*, 1969; *McCormick and Veiga*, 1992; *Trepte and Hitchman*, 1992; *Kinnison et al.*, 1994; *Boering et al.*, 1994, 1995, 1996; *Hintsa et al.*, 1994; *Avallone and Prather*, 1996; *Grant et al.*, 1996; *Minschwaner et al.*, 1996; *Volk et al.*, 1996]. The "leaky tropical pipe" model was developed in response to these studies and allows for limited exchange across the subtropical barrier [*Neu and Plumb*, 1999].

According to the leaky tropical pipe model, air can enter the midlatitude lower stratosphere either from above, by subsidence associated with the mean meridional circulation, or quasihorizontally from the tropics, by sideways advection resulting from the divergence of tropical vertical velocities or by isentropic mixing resulting from breaking of planetary or synoptic scale waves. Measurements of long-lived trace species in the midlatitude lower stratosphere are therefore potentially powerful tools for diagnosing transport rates throughout the stratosphere, since tracer mixing ratios depend on the timescales and relative importance of each of these mechanisms.

Carbon dioxide is an excellent tracer for studying the transport history of air in the midlatitude lower stratosphere. *Boering et al.* [1994, 1995, 1996] showed that the propagation of the seasonal cycle and the long-term increase in concentrations of CO_2 from the troposphere into the stratosphere provides information about transport occurring on short (weeks to months) and long (years) timescales, respectively. We show here that interannual variations in the growth rate of CO_2 also propagate into the midlatitude lower stratosphere, giving information about transport processes operating on intermediate timescales. These interannual variations, in combination with the trend and the seasonal cycle, provide sufficient information for deriving detailed age spectra. The derived age spectra quantitatively reflect the relative amounts of air entering this region by quasihorizontal transport from the tropics versus subsidence from higher altitudes.

The stratospheric age spectrum was first rigorously defined by *Hall and Plumb* [1994], who, following *Kida* [1983], recognized that an air parcel in the stratosphere is comprised of smaller fluid elements with diverse transport histories from the tropical tropopause, where most air enters the stratosphere. In other words, there is no single timescale which describes the time since an air parcel entered the stratosphere. The age spectrum $G(t, P; P_o)$ is a probability distribution function of transit times from point P_o, the tropical tropopause, for an air parcel at a point P in the stratosphere. The most probable transit time is called the modal time τ_M and corresponds to the peak of the age spectrum. The mean age Γ represents the average transit time, the first moment of the age distribution:

$$\Gamma(P;P_o) = \int_0^\infty tG(t,P;P_o)dt \,. \tag{1}$$

The width Δ of the age spectrum reflects the difference between the mean age and the modal time:

$$\Delta^2(P;P_o) = \tfrac{1}{2}\int_0^\infty (t-\Gamma(P;P_o))^2 G(t,P;P_o)dt \,. \tag{2}$$

For an inert tracer with a linearly increasing source, the stratospheric mean age is equivalent to the lag time between the occurrence of a particular mixing ratio at the tropical tropopause and the same mixing ratio at point P. Several studies have shown that under some circumstances, accurate mean ages can be derived from observations of CO_2 [e.g., *Bischof et al.*, 1980, 1985; *Schmidt and Khedim*, 1991; *Boering et al.*, 1996] and SF_6 [e.g., *Maiss et al.*, 1996; *Harnisch et al.*, 1996; *Elkins et al.*, 1996; *Volk et al.*, 1997; *Strunk et al.*, 2000].

The age spectrum can also be defined as the transfer function relating the time series of tracer mixing ratios at the tropical tropopause $n(P_o,t)$ to the time series of tracer mixing ratios at point P in the stratosphere $n(P,t)$ such that

$$n(P,t) = \int_0^t n(P_o,t-t')G(t',P;P_o)dt' \,, \tag{3}$$

where t' represents the transit time from P_o to P [*Hall and Plumb*, 1994]. In a mathematical model, the age spectrum G is equivalent to the Green's function. Knowledge of G allows us to calculate the concentration of any conserved gas if the time history of its mixing ratio is known at the tropical tropopause. In this study we invert (3) to solve for G, given a stratospheric boundary condition for CO_2 and a time series of in situ observations of CO_2 in the lower stratosphere from 1992 to 1998 obtained using the NASA ER-2 aircraft. Following *Hall and Plumb* [1994], we assume that G is independent of season or year. The consequences of this assumption for our analysis are addressed in detail below.

We found that bimodal age spectra throughout the midlatitude lower stratosphere produce simulated time series of CO_2 mixing ratios that fit observations significantly better than age spectra consisting of a single peak. The two peaks are distinct, with the mean age of the younger peak increasing with altitude from the tropopause to ~1 year for air representative of ~19.5 km at 40°N. The mean age of the older peak is 5 - 6 years throughout this altitude region. The older peak accounts for ~10% of the area of the age spectrum at ~14.5 km, increasing to ~50% at 19.5 km. We argue that the younger peak represents rapid quasihorizontal transport of air from the tropics, while the older peak represents downwelling of air from higher altitudes in the mean meridional circulation. The mean ages of the younger and older peaks in the derived age spectra provide estimates of the residence times for air in the lower and middle stratosphere, respectively, and the separation of the peaks implies a significant altitude region where there is little meridional exchange between the tropics and midlatitudes.

The recent NASA "Models and Measurements II" (MMII) study revealed a large discrepancy between mean ages predicted by the majority of two-dimensional (2-D) and 3-D models of the atmosphere and those derived from observations of SF_6 and CO_2, with most models significantly underestimating mean ages compared to observations [*Park et al.*, 1999; *Hall et al.*, 1999]. Several studies have investigated factors controlling mean age in these models and the implications for predicting the stratospheric response to natural or anthropogenic perturbations [*Bacmeister et al.*, 1998; *Fleming et al.*, 1999; *Li and Waugh*, 1999; *Hall and Waugh*, 2000], but uncertainties regarding the nature and significance of this discrepancy remain.

Hall and Plumb [1994] and *Hall and Waugh* [1997] showed that age spectra provide a useful framework for diagnosing and comparing transport schemes in models, and a comparison of model age spectra was included in MMII [*Park et al.*, 1999]. *Schoeberl et al.* [2000] extended the age spectrum formalism to a Lagrangian frame of reference and considered the relationship between the age spectrum and abundance for tracers with stratospheric sinks. They postulated that the mean age of an air parcel may be sensitive to a small amount of very old air that would have only a slight impact on the mixing ratio of a reactive tracer, so that using mean age as a major criterion for evaluating model transport may be inappropriate. However, until recently, there has been no information available about age spectra in the real atmosphere, so it is not known whether mean ages derived from SF_6 and CO_2 are in fact strongly affected by a small amount of very old air.

In an earlier paper we derived age spectra for the lower tropical stratosphere using vertical profiles of CO_2 [*Andrews et al.*, 1999]. *Johnson et al.* [1999] attempted to obtain age spectra for several altitudes in the tropics and at 30°N using balloon and satellite observations of H_2O and CH_4, but their analysis was complicated by the lack of well-defined stratospheric boundary conditions for these species and the subtlety of the signal they were attempting to recover (the reported long-term increase in stratospheric H_2O mixing ratios). The empirical age spectra presented here provide quantitative insight into transport rates throughout the stratosphere and into the source of the discrepancies between modeled and "measured" mean age. *Jones et al.* [this issue] show how the derived age spectra can be used to constrain proposed transport mechanisms in a 2-D model and conclude that in their model the relative rates of meridional transport in the lower and middle stratosphere determine the separation of the two peaks in the age spectrum and the overall mean age of air in the lower stratosphere.

2. Observations

Variations in CO_2 at a particular altitude in the stratosphere represent both the propagation of temporal variations from the troposphere and reversible displacement of tracer isopleths associated with planetary scale waves [*Ehhalt et al.*, 1983; see, e.g., *Boering et al.*, 1996, Figure 1]. To minimize the impact of reversible displacements and to provide an optimum framework for comparing observations from different latitudes, we assess temporal changes in CO_2 referenced to a long-lived tracer, N_2O, which is in effect the vertical coordinate for this analysis (see discussion below). Our results can be mapped onto a latitude/height coordinate system using the seasonally resolved climatology of N_2O from in situ observations compiled by *Strahan et al.* [1999]. Similarly, we used equivalent latitude [*Nash et al.*, 1996] to identify air with midlatitude character, instead of using latitude. Equivalent latitude is a coordinate based on potential vorticity (PV), which is nearly conserved on timescales typical of reversible wave transport.

Simultaneous in situ measurements of CO_2 and N_2O were obtained using the NASA ER-2 aircraft during 19 deployments between November 1992 and November 1998. Field campaigns included the Stratospheric Photochemistry and Dynamics Expedition (SPADE, 1992-1993, 14°N to 61°N), the Airborne Southern Hemisphere Ozone Experiment/Measurements for Assessing the Effects of Stratospheric Aircraft (ASHOE/MAESA, 1994, 70°S to 61°N), Stratospheric Tracers of Atmospheric Transport (STRAT, 1995-1996, 3°S to 61°N), Photochemistry of Ozone Loss in the Arctic Region in Summer (POLARIS, 1997, 2°S to 90°N), and a short test flight series in November 1998 (11°N to 37°N). Measurements were obtained up to the maximum altitude of the ER-2 (~21 km). Deployments occurred in all seasons except Southern Hemisphere summer. Northern Hemisphere midlatitude data were obtained during 15 deployments.

CO_2 was measured by nondispersive infrared absorption with a long-term precision better than 0.1 ppmv [*Daube et al.*, A high-precision fast-response airborne CO_2 analyzer for in situ sampling from the surface to the middle stratosphere, manuscript in preparation; *Boering et al.*, 1994, 1996]. Simultaneous observations of CH_4 from the Airborne Laser Infrared Absorption Spectrometer (ALIAS) [*Webster et al.*, 1994] are used to account for stratospheric production of CO_2 by oxidation of CH_4, assuming that differences between observed CH_4 and the tropospheric value (≅1725 ppbv) represent oxidation to CO_2. The CH_4 correction is small but significant for this analysis (≅0.35 ppmv for N_2O = 230 ppbv).

N_2O was measured by the Airborne Tunable Laser Absorption Spectrometer (ATLAS) as described by *Podolske and Loewenstein* [1993]. During ASHOE/MAESA, STRAT, and POLARIS, uncertainty in reported N_2O ratios was 3.5%, but during SPADE, the estimated uncertainty was 7% [*Strahan et al.*, 1999]. We corrected for growth in the tropospheric mixing ratio of N_2O from 1992 to 1997 by scaling data from each flight by a factor of $1.0020^{(1997-t)}$, where t is the flight date in years, following *Strahan et al.* [1999]. This factor is based on the average trend of 0.20%yr^{-1} observed in surface measurements of N_2O from 1987 to 1997 [*U.S. Department of Commerce*, 1996]. We have limited this analysis to air with $N_2O \geq 235$ ppbv, since seasonal variations of CO_2 are too small to detect at higher altitudes and to exclude measurements obtained in remnants of the polar vortex encountered at midlatitudes.

Measurements of temperature, pressure and position were made by the Meteorological Measurement System on board the ER-2 [*Scott et al.*, 1990]. Uncertainties for temperature and pressure are 0.3 hPa and 0.3 K, respectively These measurements are used to calculate potential temperature θ with an uncertainty of 2-3 K. For this analysis we selected air with $\theta \geq 390$ K, to exclude the "stratospheric middleworld" or "lowermost stratosphere," the region between the tropopause and $\theta = 390$, where air parcels can travel from the troposphere to the stratosphere isentropically [*Holton et al.*, 1995].

The calculation of equivalent latitude is described in detail by *Strahan et al.* [1999]. For each flight date, potential vorticity from analyses by the National Center for Environmental Prediction (NCEP) were mapped onto an equal area grid and the area enclosed by each isoline was determined. For a particular value of PV on an isentrope, the equivalent latitude corresponds to the latitude with poleward area equal to the area enclosed by the same PV isoline if distributed symmetrically about the pole. Equivalent latitude was mapped onto the ER-2 flight track via the PV analyses, using relationships between equivalent latitude, PV, and potential temperature. For days where the NCEP analyses were not available, potential vorticity was obtained from the Goddard Data Assimilation Office GEOS 1 analyses. For this study we selected data with 35°N ≤ equivalent latitude ≤ 55°N.

3. Analysis

We seek to invert (3) to solve for $G(t,P;P_o)$ given measurements of the stratospheric boundary condition for CO_2, $CO_2(P_o,t)$ and the concentrations in the midlatitude lower stratosphere, $CO_2(P,t)$. We first derived a continuous representation of $CO_2(P_o,t)$ (Figure 1), as discussed by *Andrews et al.* [1999]. If temporally and spatially continuous data were available, we could simply compute an average CO_2 time se-

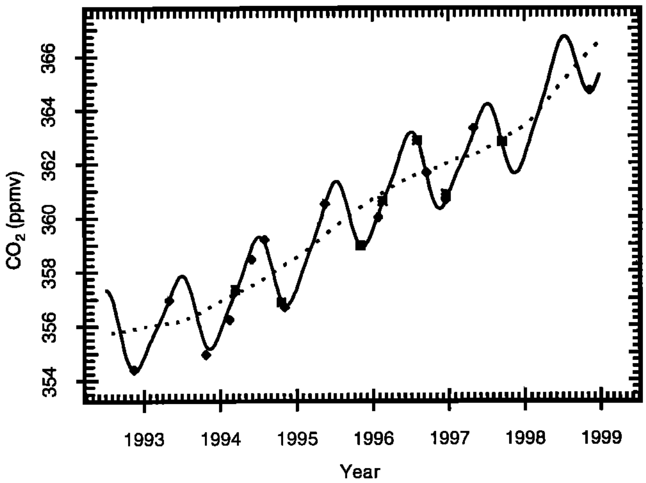

Figure 1. Boundary condition for CO_2 entering the stratosphere. Data collected in the tropics are shown as asterisks, while the diamonds represent data obtained when the ER-2 intercepted an air mass with tropical character (as determined by simultaneous observations of N_2O and H_2O) in the extratropics. The dotted curve represents the 12-month running mean of the average of surface data from the National Oceanic and Atmospheric Administration Climate Monitoring and Diagnostics Laboratory flask network stations at Mauna Loa and Samoa [*Conway et al.*, 1994] (updated) delayed by 2 months. The solid line is the sum of the dotted line and a two-harmonic representation of the seasonal cycle in CO_2 mixing ratios in air entering the stratosphere given by $CO_2^{seas} = 0.007 + 1.490 \sin(2\pi t - 1.244) + 0.328 \sin(4\pi t + 0.766)$ where t is time in years. Additional details are given by *Andrews et al.* [1999].

ries for a given point P in the stratosphere. However, while our stratospheric observations have extensive latitudinal coverage during 15 deployments over a 6-year period, the observations are limited with respect to longitude, and each deployment typically lasted only 2 - 4 weeks. Thus the data are undersampled both spatially and temporally. Fortunately, we can substantially reduce uncertainty due to undersampling (as well as account for variability due to reversible displacements of air, as noted earlier) by exploiting the compact relationships between mixing ratios of CO_2 and N_2O at ER-2 altitudes in midlatitudes. Our results can be mapped back into the latitude/height domain using the climatology of N_2O observations from ER-2 data given by *Strahan et al.* [1999] and an average relationship between potential temperature and height derived from NCEP analyses.

Boering et al. [1994, 1996] and *Strahan et al.* [1998] have shown previously that relationships between CO_2 and N_2O are remarkably compact in the midlatitude lower stratosphere and that the propagation and attenuation of the CO_2 seasonal cycle from the troposphere can be clearly delineated when the CO_2 data are binned with respect to N_2O. *Ehhalt et al.* [1983] first noted that variations of certain long-lived trace species are correlated, in an analysis of data from midlatitude balloon flights, and they attributed the observed covariance to coherent, reversible deformation of tracer isopleths. *Plumb and Ko* [1992] extended this result to the global scale, showing that compact relationships among tracers exist when the timescales for horizontal transport are much faster than the local photochemical lifetime. Data for CO_2 and N_2O for air with θ > 390 K and 35°N ≤ equivalent latitude ≤ 55°N are shown in Figure 2 for 15 time periods between 1992 and 1998, illustrating the compact relationships observed throughout Northern Hemisphere midlatitudes.

An advantage of performing the analysis with N_2O as the vertical coordinate is that, to a large extent, N_2O and "age" are affected similarly by seasonal and interannual (e.g., the quasibiennial oscillation) variations in stratospheric transport rates. We are therefore able to obtain good fits to the observations without having to account for this type of variation. A disadvantage is that the results are more difficult to interpret in terms of actual velocities, since the location of N_2O isopleths varies seasonally. Furthermore, we must verify that binning the data with respect to N_2O mixing ratio does not bias our results. This question is discussed in detail in section 4.4.

A number of numerical methods have been developed for solving Fredholm equations like (3), but most methods require that the observations $n(P,t)$ be evenly spaced (e.g., Fourier analysis). The stratospheric CO_2 signal is quite complex, with a seasonal cycle superimposed on an increasing trend that exhibits significant interannual variability. The temporal resolution of the in situ data (15 time points in 6 years) is not adequate to completely define this complex signal, so the data cannot be interpolated onto an evenly spaced temporal grid. We chose to approach the problem by choosing a functional form for the age spectrum on an N_2O isopleth, $G(t, N_2O; P_o)$, and using a genetic algorithm, a powerful optimization technique modeled on the theory of natural selection, to identify the optimal coefficients of the function.

In our derivation of empirical age spectra for the tropical lower stratosphere from observations of CO_2 [*Andrews et al.*, 1999], we used a functional form based on the analytic solution for the Green's function of the 1-D diffusion equation [*Hall and Plumb*, 1994]. We adopted the same functional form for this analysis,

$$G(t, \mathrm{N_2O}; P_o) = \frac{N(\mathrm{N_2O})}{\sqrt{t^3}} \exp\left(-B(\mathrm{N_2O})t - \frac{C(\mathrm{N_2O})}{t} \right), \quad (4)$$

where t represents the transit time from the tropical tropopause P_o (equivalent to $N_2O \cong 310$ ppbv), N is defined so that the function has unit area, and B and C are functions of N_2O. This function has many of the characteristics of age spectra generated by more realistic 2-D and 3-D models (T. M. Hall and D. W. Waugh, personal communication, 1998), suggesting that its usefulness extends beyond the 1-D framework. Because transport into the midlatitude lower stratosphere is potentially more complicated than transport in the tropical lower stratosphere, we also performed the analysis using a more flexible functional form consisting of two peaks:

$$G(t, \mathrm{N_2O}; P_o) =$$

$$A_1(\mathrm{N_2O}) \frac{N_1(\mathrm{N_2O})}{\sqrt{t^3}} \exp\left(-B_1(\mathrm{N_2O})t - \frac{C_1(\mathrm{N_2O})}{t} \right) +$$

$$(1 - A_1(\mathrm{N_2O})) \frac{N_2(\mathrm{N_2O})}{\sqrt{t^3}} \exp\left(-B_2(\mathrm{N_2O})t - \frac{C_2(\mathrm{N_2O})}{t} \right) \quad (5)$$

where N_1 and N_2 are chosen so that each peak has unit area and A_1 determines the relative contribution of each peak. This functional form can generate age spectra consisting of two

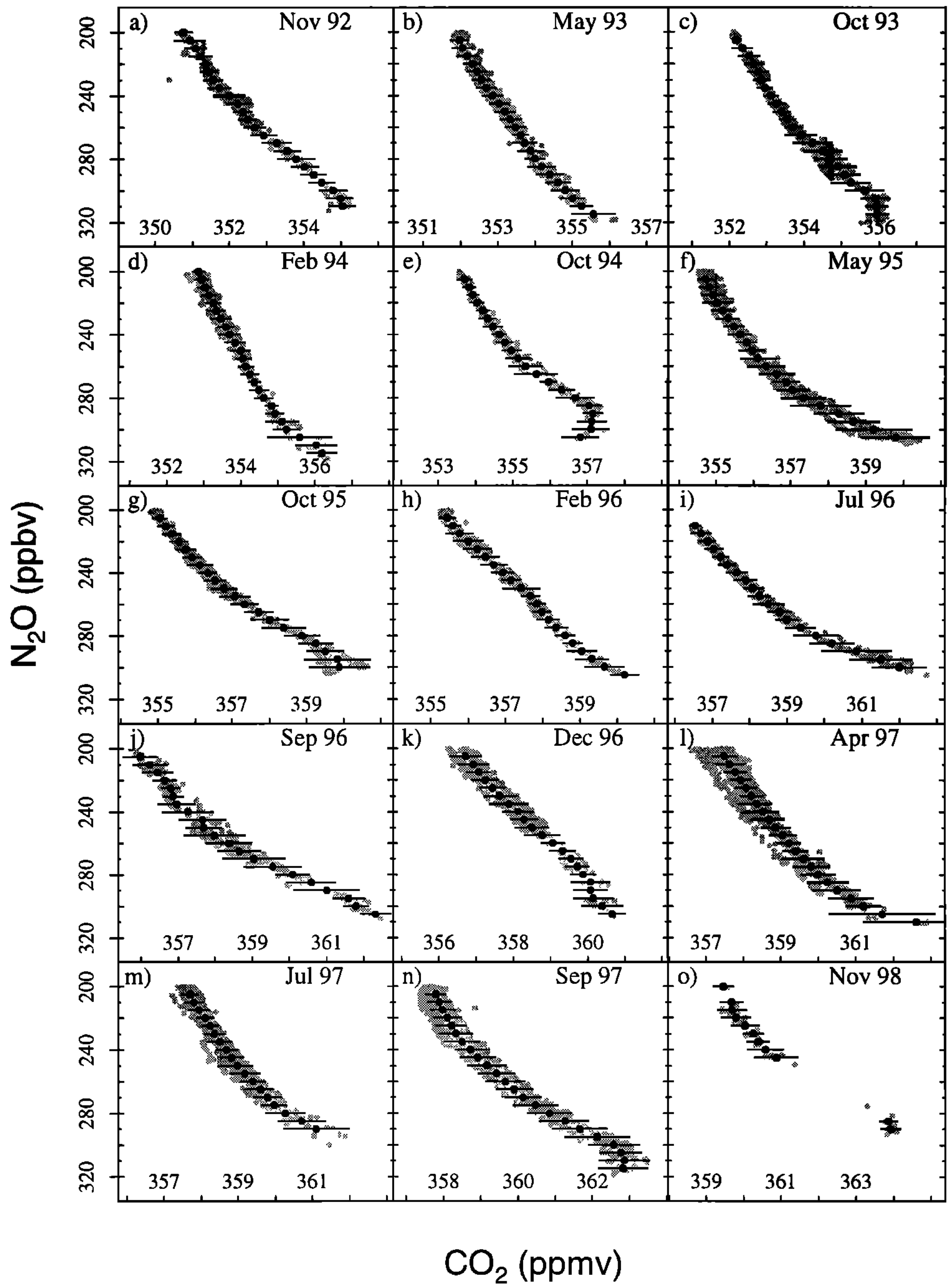

Figure 2. Observations of CO_2 and N_2O for air with equivalent latitude 35°-55°N and potential temperature > 390 K. Lightly shaded points are 10-s averages of the flight data. Solid circles represent the mean CO_2 and N_2O mixing ratio binned with respect to N_2O in 24 overlapping 10 ppb intervals then interpolated onto an evenly spaced grid in N_2O. Error bars correspond to 2 standard deviations of the mean.

distinct peaks, a single wide peak, or a single peak with a long tail. It provides excellent fits to age spectra generated by state-of-the-art 2-D and 3-D models of stratospheric transport. Finally, to test the sensitivity of our results to the functional form, we used a crude function constructed of two "boxcar" functions, characterized by the average transport time and width (see Figure 3 for examples) of each peak plus the relative contribution of each peak to the total (unit) area. Both the bimodal exponential function (equation (5)) and the dual boxcar functions therefore have five adjustable parameters.

Optimization of the parameters was accomplished using a genetic algorithm [*Holland*, 1975], a scheme modeled after the theory of evolution that has been applied to many problems in geophysics [e.g., *King*, 1995; *Conway and Bland*, 1998]. Due to the nonlinearity of our problem and the need to optimize five parameters, it is difficult to solve by simpler methods, like least squares. The bimodal functions are also degenerate (composed of identical functional forms). Monte Carlo techniques are potentially applicable, but in this case are too time consuming to be practical. Like Monte Carlo

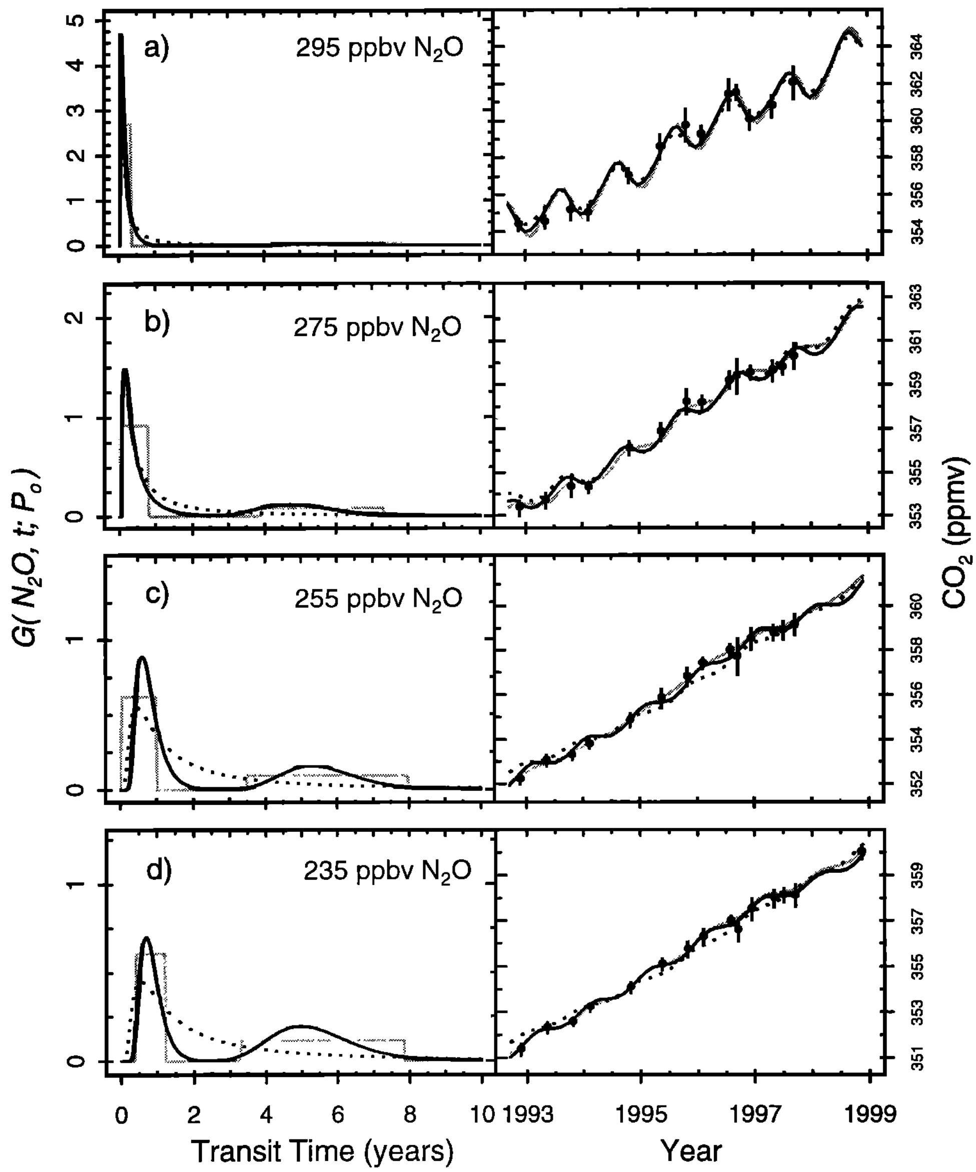

Figure 3. Optimum age spectra for (a) 295, (b) 275, (c) 255, and (d) 235 ppbv N_2O for the single-peaked (dotted), 1-D bimodal (dark solid) and bimodal boxcar (light solid) functional forms shown with the corresponding CO_2 time series. Symbols represent the CO_2 mixing ratios from Figure 2 with 2σ error bars, corrected for stratospheric production by CH_4 oxidation using simultaneous measurements of CH_4 [*Webster et al.*, 1994].

methods, genetic algorithms use stochastic exploration of parameter space, but a genetic algorithm acquires and retains information about the solution space, making it much more efficient for problems with many parameters. The algorithm developed for this work is described in the Appendix.

4. Results and Discussion

4.1. Optimum Age Spectra

The optimal age spectra derived for several N_2O surfaces are shown in Figure 3, along with the corresponding CO_2 observations and the time series of CO_2 generated from the derived age spectra. At all N_2O values the optimal age spectra with two peaks generate CO_2 time series that have a significantly lower root-mean-square (rms) error with respect to the CO_2 observations than do age spectra consisting of a single peak. Over much of the N_2O range, the rms error is a factor of 2 lower for the bimodal age spectra (Figure 4). The variation with respect to N_2O of mean age and modal time are shown in Figure 5 for each peak of the bimodal age spectra, along with the overall mean age (the first moment of the bimodal age distribution). The similarity of the solutions obtained for the 1-D bimodal and the bimodal boxcar cases is apparent from Figures 3 and 4. Detailed comparison reveals that the fundamental parameters of these solutions are essentially identical (Figures 6 and 7). Thus our results are apparently not overly sensitive to the functional form of the age spectrum.

Note that we also tested a functional form for the age spectrum comprised of three peaks. Results using this func-

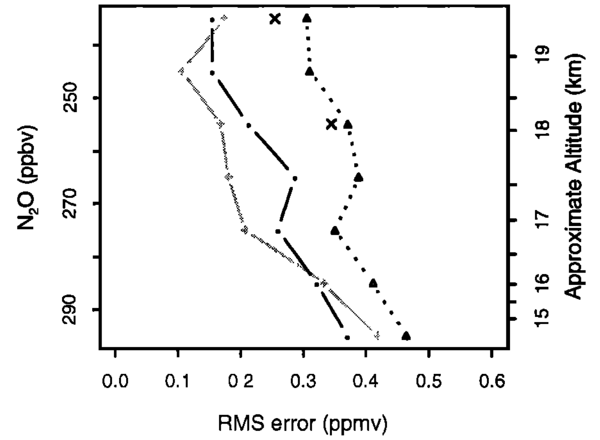

Figure 4. Variation with N_2O of the CO_2 root-mean-square (rms) error corresponding to the optimum age spectra for the single-peaked (dotted line with triangles), 1-D bimodal (dark solid line with solid circles) and bimodal boxcar (light solid line with plus symbols) functional forms. Crosses indicate results from the Harvard 2-D model. For the purposes of this analysis, CO_2 rms error = $(\Sigma(CO_2^{obs} - CO_2^{spec})^2/N)^{(1/2)}$, where CO_2^{obs} and CO_2^{spec} denote observed and predicted CO_2 mixing ratios, respectively, and N is the number of observations. The relationship between N_2O and approximate altitude was derived using an annual average relationship between N_2O and potential temperature from *Strahan et al.* [1999] and an annual average relationship between potential temperature and altitude from NCEP analyses.

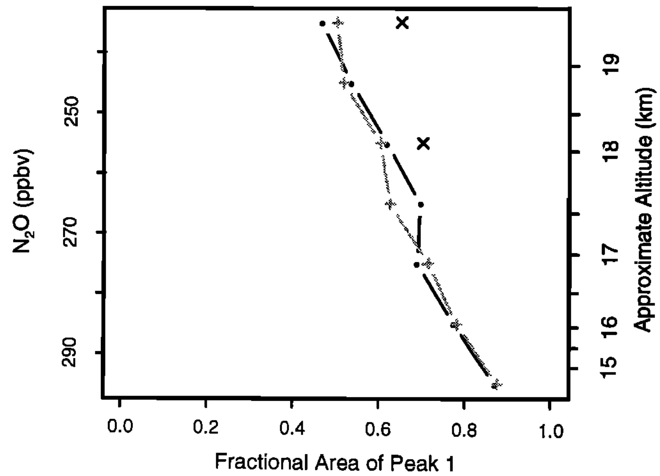

Figure 6. Fraction of the area of the age spectrum associated with the younger peak for the 1-D bimodal (dark solid line with solid circles) and bimodal boxcar (light solid line with plus symbols) functional forms. Crosses indicate results from the Harvard 2-D model.

tion were more variable than for the bimodal functional form because there was not enough information in the data to adequately constrain all the parameters. The optimal solutions using the trimodal function were not substantially different than the optimal bimodal solutions, suggesting that the bimodal function captures the salient features of the data. Furthermore, the CO_2 rms errors for the trimodal functions were not significantly lower than for the corresponding bimodal functions, demonstrating that the goodness of fit cannot be infinitely increased by continuing to add degrees of freedom.

Figure 5. Variation with N_2O of the mean age (solid circles) and modal time (plus symbols) of the younger peak (dark) and the older peak (light) for the bimodal functional form based on the solution to the 1-D diffusion equation. The overall mean age (the first moment of the bimodal distribution) is also shown (inverted triangles).

An important result of this analysis is that the mean age of the air on an N_2O isopleth is the same for all three functional forms (Figure 7b). For air younger than ~2 years (N_2O > ~275 ppbv), the persistence of the CO_2 seasonal cycle and of interannual variations in the growth rate introduces significant errors if mean age is calculated by computing the lag time relative to the mean linear trend (we will refer to mean ages derived in this way as "CO_2 lag times"). Mean ages derived from SF_6 are similarly subject to errors due to uncertainties in the boundary condition, nonlinearity in the growth rate, and the limits of measurement precision [*Volk et al.*, 1997; *Ray et al.*, 1999]. The mean ages derived from the age spectra are in good agreement with the average relationship between N_2O and CO_2 lag times calculated from ER-2 measurements obtained during many seasons from 1992 to 1998 (Figure 7b). We conclude that the relationship between N_2O and mean age from the midlatitude age spectra provides accurate mean ages for midlatitude air with N_2O > 235 ppbv and likely represents the most accurate method currently available for determining the age of midlatitude air near the tropopause (N_2O > 275 ppbv).

Inspection of Figure 3 shows that neither the single-peaked or the bimodal age spectra are characterized by a substantial amount of very old air. For the bimodal age spectra, air older than 10 years makes a negligible contribution to mean age at the altitudes considered in this study. However, for the single-peaked spectra, neglecting air older than 10 years when calculating mean age produces values that are 20 - 30% younger than the true mean age.

The temporal evolution of CO_2 mixing ratios on selected N_2O isopleths is shown in Plate 1. These results are consistent with observations that seasonal extrema in CO_2 and H_2O mixing ratios are observed at midlatitudes latitudes within 1-2 months of their occurrence in the tropics [*Boering et al.*, 1994, 1995, 1996; *Strahan et al.*, 1998; *Hintsa et al.*, 1994]. Even at 235 ppbv N_2O (~19.5 km, Γ ~3.25 years) there is still evidence of the seasonal cycle propagating from the tro-

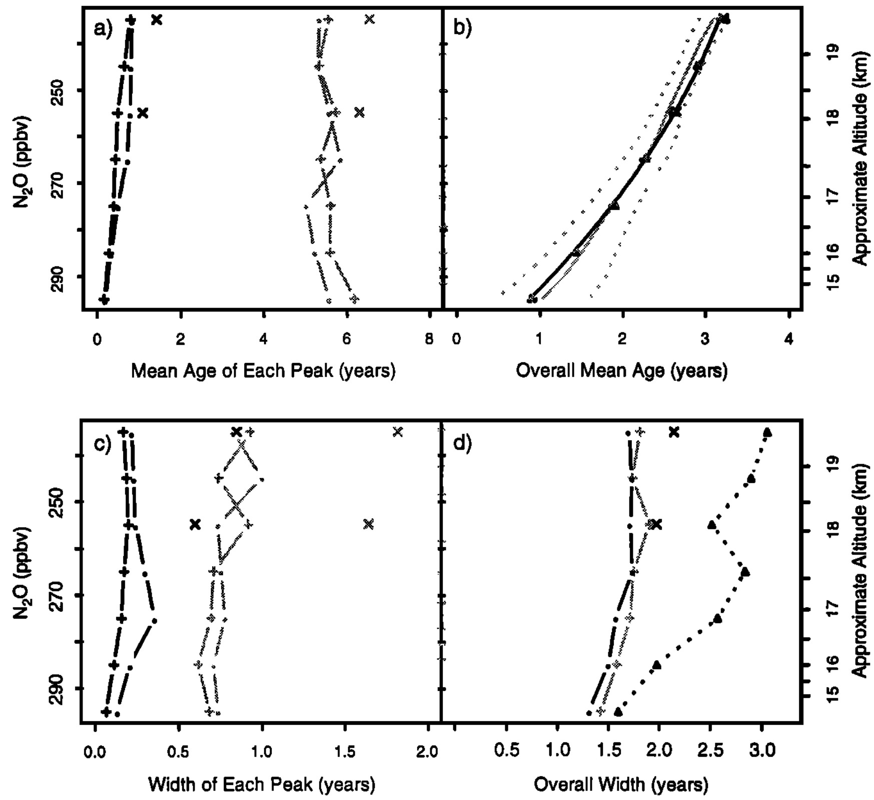

Figure 7. (a) Comparison of the mean ages of the individual peaks for the 1-D bimodal (solid circles) and the bimodal boxcar (plus symbols) cases. Dark (light) symbols correspond to the younger (older) peaks. Crosses denote results from the Harvard 2-D model. (b) Overall mean age as a function of N_2O for the three functional forms used in the analysis. Symbols are the same as in Figure 7a, with the addition of results from the 1-D single-peaked case (open triangles). Light solid curve represents average lag time calculated from ER-2 CO_2 observations obtained from 1992 to 1998 for the latitude range 35°-55°N. Light dotted lines denote the range of values within 1σ of the mean. Dark solid curve is a quadratic fit to the 1-D bimodal results given by $\Gamma = 0.0566(313 - N_2O) - 0.000195(313 - N_2O)^2$. (c and d) Same as Figures 7a and 7b but for spectral width.

posphere. The peak-to-peak amplitude of the signal at 235 ppbv is 0.3 - 0.4 ppm, and the phase lag time for the seasonal extrema is 0.7 - 0.8 year.

Midlatitude data from the Southern Hemisphere were not included in the optimization but are nevertheless fit reasonably well by the resulting CO_2 time series (open triangles in Plate 1), consistent with results from *Boering et al.* [1996] showing that seasonal variations in CO_2 in the NH and SH lower stratosphere are in phase. Agreement is especially good for air with 295 ppbv N_2O and with $N_2O \leq 245$ ppbv.

The most pronounced disagreements between the observations and CO_2 mixing ratios calculated from the optimal age spectra occur for the September 1996 deployment. This deployment was unusually short (data included in the analysis were obtained on only three flights), so it is possible that the values are not truly representative of the mean midlatitude CO_2:N_2O relationship for this period. Although the November 1992 and November 1998 deployments were also quite short (two flights), isentropic mixing by planetary scale waves is more effective in November, resulting in more homogeneous tracer distributions, as evidenced by the smaller variances observed (see Figure 2). Another possibility is that the PV analysis for one or more of the September flights failed to identify a filament of tropical or high-latitude air.

To evaluate the significance of our results, it is important to determine what feature of the CO_2 data is better fit by bimodal age spectra compared to the unimodal spectra. The complicated temporal variation of CO_2 makes it uniquely well suited for determining age spectra. The long-term increase due to fossil fuel combustion gives information about the mean age of the spectrum, and the phase lag and amplitude attenuation of seasonal variations provide detailed insight into transport processes occurring on timescales from a few weeks to several months. Additionally, Fourier analyses of the CO_2 records from Mauna Loa and South Pole [*Keeling and Whorf*, 1994] reveal low-frequency harmonics at ~0.1 yr^{-1} and 0.26 yr^{-1}. Possible sources of these oscillations are discussed by *Keeling et al.* [1995]. The long-period oscillations are included in our representation of the stratospheric boundary condition for CO_2, where they appear as deviations from a linear trend (Figure 8).

Based on simulations performed using the Goddard Institute for Space Studies global climate/middle atmosphere model (GCM), *Hall and Prather* [1993] hypothesized that such interannual variations in the CO_2 growth rate would propagate into the stratosphere. Our time series of CO_2 and N_2O observations in the stratosphere shows for the first time that these long-period oscillations are present in stratospheric

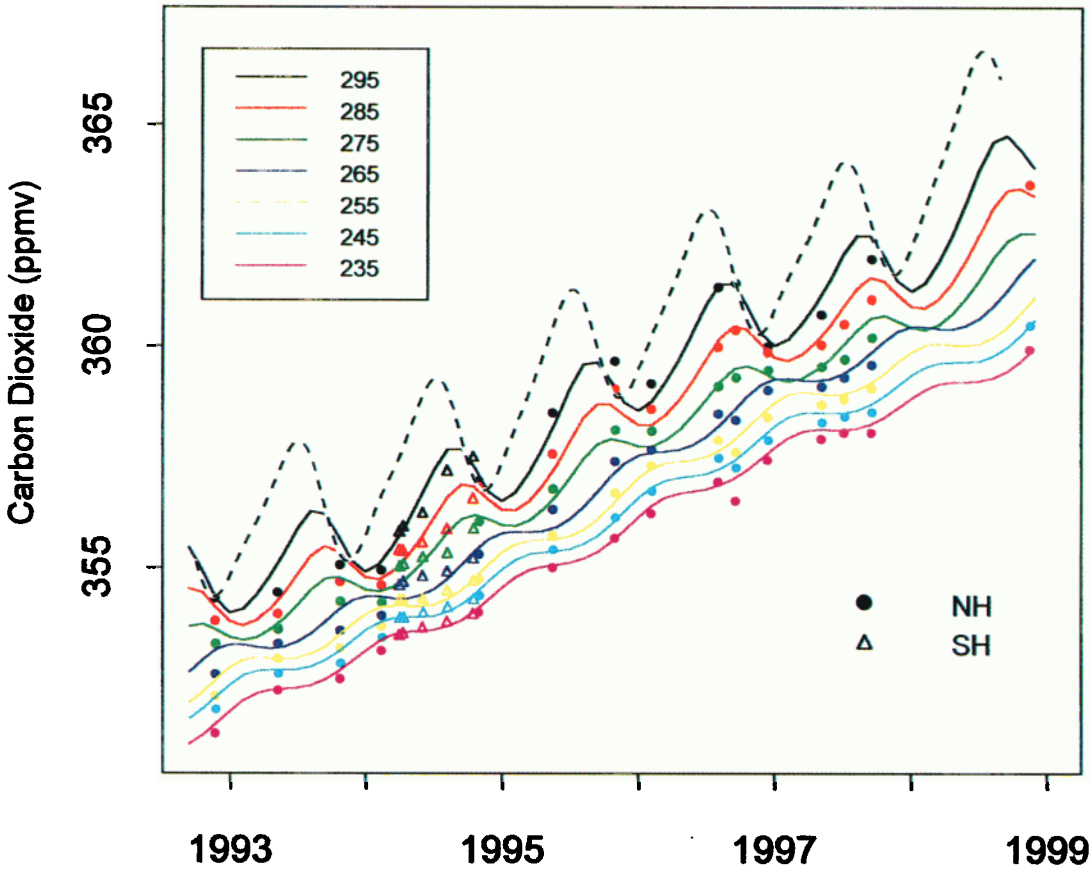

Plate 1. Temporal evolution of CO_2 on N_2O isopleths at NH midlatitudes corresponding to the 1-D bimodal empirical age spectra (solid lines). Stratospheric boundary condition is also shown (dotted line). Symbols represent the CO_2 mixing ratios from Figure 2, corrected for stratospheric production by CH_4 oxidation using simultaneous measurements of CH_4 [*Webster et al.*, 1994]. Data from the Southern Hemisphere midlatitudes are shown as triangles; these data were not used in the optimization.

air at relatively high altitudes (up to ~18.5 km), with very little phase delay (Figure 9). This is a surprising result indicating that at least some air must be transported rather quickly to the given location from the tropical tropopause, and it places strong constraints on the shape of proposed age spectra for transit times ranging from several months to several years. The age spectra consisting of a single peak evidently do not have enough degrees of freedom to simultaneously capture these interannual variations in the growth rate, the phase and amplitude of the seasonal cycle, and the mean age.

4.2. Implications for Stratospheric Transport

One interpretation of the clear separation of the two peaks in our bimodal age spectra is that there are two predominant routes by which air enters the midlatitude lower stratosphere. The younger peak results from rapid quasihorizontal transport from the tropics, due to both mean motions and to eddies, while the older peak represents transport by the mean residual circulation, through which air rises to high altitudes in the tropics and descends at higher latitudes. The relative areas of the two peaks reflect the importance of each pathway. For the age spectrum to consist of two distinct peaks, there must be a region within a few kilometers of the tropopause where quasihorizontal transport from the tropics to higher latitudes occurs rapidly, and there must also be a significant altitude region above the rapid-transport layer where there is little meridional exchange across the subtropics (either into or out of the tropics). The permeability and height of this subtropical "barrier" to horizontal transport determines the extent to which the peaks are separated.

Previous studies provide considerable support for this picture of stratospheric transport. The distribution of debris from the tropical nuclear bomb tests in the late 1950s [*Feely and Spar*, 1960; *Telegadas and List*, 1969; *Kinnison et al.*, 1994] and aerosols from tropical volcanic eruptions [e.g., *Trepte and Hitchman*, 1992; *McCormick and Veiga*, 1992; *Deshler et al.*, 1993; *Trepte et al.*, 1993; *Grant et al.*, 1996] indicate that there is limited transport of air from the tropics to midlatitudes for altitudes from ~21-28 km, whereas poleward transport across the subtropics occurs more readily within a few kilometers of the tropopause. Similarly, *Boering et al.* [1994, 1995, 1996] and *Hintsa et al.* [1994] argued that rapid propagation of the seasonal cycles in CO_2 and water vapor indicate significant poleward flow of air from the tropics near the tropopause, with slower exchange across the subtropical zone at higher altitudes, and *Strahan et al.* [1998] used the attenuation of the CO_2 cycle transported to midlatitudes to conclude that transport of tropical air to midlatitudes weakens with height in the lower stratosphere. Furthermore, vertical profiles of tracers with stratospheric sinks (e.g., N_2O, CH_4, $CFCl_3$) obtained in the tropics from aircraft, satellites, and

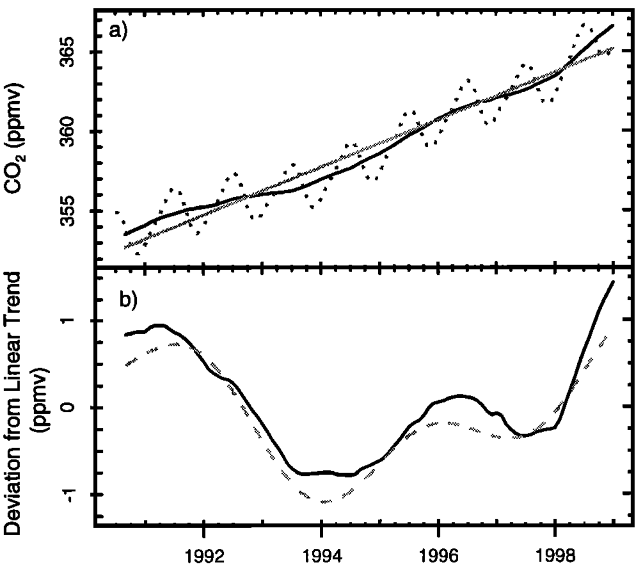

Figure 8. (a) The stratospheric boundary condition for CO_2 (dotted line). The dark line is the 12-month running mean of the boundary condition, and the light straight line is a linear fit to the boundary condition. (b) The difference between the 12-month running mean of the boundary condition and the linear fit (dark solid line) and a fit to this difference including 0.26 yr^{-1} and 0.1 yr^{-1} harmonics (light dashed line).

balloons appear consistent with greater transport of air from midlatitudes below ~21 km than above [*Minschwaner et al.*, 1996; *Volk et al.*, 1996; *Herman et al.*, 1998], and *Mote et al.* [1998] found a broad minimum near 22 km in the rate for mixing of midlatitude air into the tropics, using a simple model constrained by satellite data for H_2O + $2CH_4$.

Evidence of a "tropical stratospheric reservoir" is apparent in latitudinal cross sections of isopleths of long-lived trace species from satellites, which are characterized by sharp gradients in the subtropics [e.g., *Randel et al.*, 1993]. Differences between the tropics and higher latitudes are also found in relationships among tracers measured using aircraft [e.g., *Murphy et al.*, 1993; *Avallone and Prather*, 1996; *Volk et al.*, 1996; *Boering et al.*, 1996; *Flocke et al.*, 1999], high-altitude balloons [*Goldan et al.*, 1980; *Herman et al.*, 1998], and satellites [e.g., *Michelsen et al.*, 1998]. The aircraft measurements, in particular, reveal sharp gradients in tracer relationships in the subtropics.

Some modeling studies have reproduced the altitude dependence of tropical-extratropical exchange implied by these data. *Chen et al.* [1994] reported greater transport of tropical air into midlatitudes at 400 K and 1100 K than at 600 K. The transport at 400 K was associated primarily with trapped synoptic-scale waves propagating from the troposphere that do not extend to 600 K. Transport at 1100 K was effected largely by vertically propagating planetary waves that increase in amplitude with decreasing density; they are much more effective at transporting tropical air to higher latitudes at 1100 K than at 600 K. Similar conclusions were obtained by *Waugh* [1996] in a more extensive study. These results are qualitatively consistent with our finding of a bimodal age spectrum.

Several studies of stratospheric dynamics indicate significant seasonal and interannual variations in transport out of the tropics, including variations in meridional transport associated with the quasibiennial oscillation (QBO) in tropical stratospheric winds [e.g., *Trepte and Hitchman*, 1992; *Waugh*, 1996; *Jones et al.*, 1998]. However, we were able to obtain good fits to the CO_2 observations on N_2O isopleths without explicitly accounting for possible temporal variation in transport rates. This is probably because distributions of CO_2 and N_2O are affected similarly by variations in transport rates.

To address temporal variations in transport rates, we can use a climatology of N_2O mixing ratios from ER-2 observations to transform our results from N_2O isopleths to geometric coordinates. *Strahan et al.* [1999] used equivalent latitude to develop seasonally resolved average distributions of N_2O from 360-530 K for the period 1987-1997. Mean midlatitude N_2O profiles calculated for each season from their results are shown in Figure 10. Mixing ratios of N_2O are ~15 ppbv lower during Northern Hemisphere (NH) winter than in NH summer for a given potential temperature, presumably because of increased downwelling due to greater wave forcing during NH winter. At 450 K this change in N_2O corresponds to a change in the mean age of ~0.4 year, while at 400 K it is ~1.2 years. *Strahan et al.* [1999] were unable to explore possible QBO effects on the distribution of N_2O due to the lim-

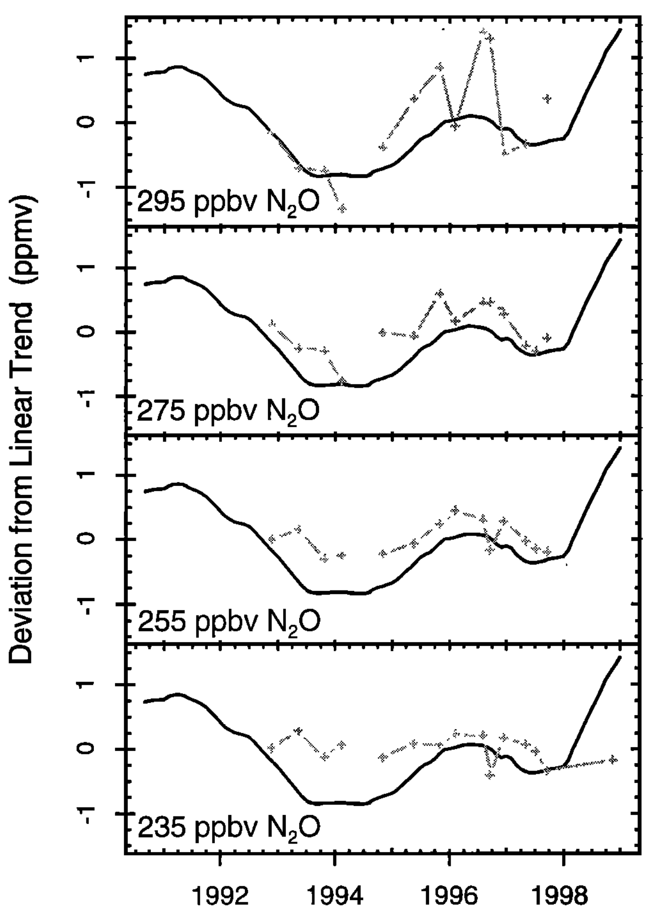

Figure 9. CO_2 observations corresponding to several N_2O isopleths detrended by subtracting the linear fit to the boundary condition then subtracting the mean of the residuals (light symbols) shown along with the deviation from the linear trend in the stratospheric boundary condition (solid line, same as dark solid line in Figure 8b.)

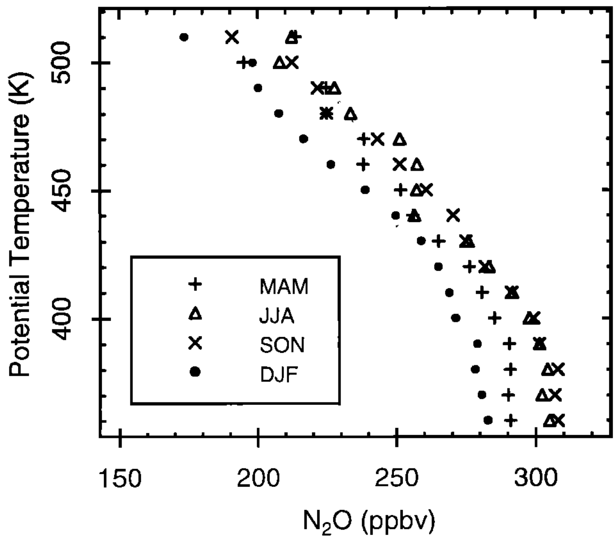

Figure 10. Seasonal variation of mean midlatitude (35°≤ equivalent latitude ≤ 55° N) N_2O from the analysis of *Strahan et al.* [1999]. MAM, March, April, May; JJA, June, July, August; SON, September, October, November; DJF, December, January, February

ited temporal and longitudinal coverage of available aircraft data.

If our interpretation of the bimodal age spectra is correct, the mean age of the older peak provides a timescale for air to be transported by the residual circulation. Furthermore, since the air comprising the older peak is assumed to have descended from above, the older peak should resemble the age spectrum at higher altitudes with modifications that occurred as the air descended. The derived ages for the older peak (5.4 ± 0 4 years) are notably similar to mean ages in the midlatitude and high-latitude middle stratosphere calculated from measurements of CO_2 and SF_6 obtained using in situ and whole air samplers on high-altitude balloons [e.g., *Andrews et al.*, Mean ages of stratospheric air derived from *in situ* observations of CO_2, CH_4 and N_2O, submitted to *J. Geophys Res.*; *Park et al.*, 1999, chap. 2; *Bischof et al.*, 1980, 1985; *Schmidt and Khedim*, 1991; *Harnisch et al.*, 1996, 1998; *Strunk et al.*, 2000] and to mean ages determined from CO_2 mixing ratios in remnants of the polar vortex sampled by the ER-2 [*Boering et al.*, 1996], as expected if the middle stratosphere is the source region for air comprising the older peak. It is reasonable to expect that the older peak would shift toward younger ages with increasing altitude, but there is no obvious trend with altitude in either the mean age or modal time of this peak in the results shown in Figure 5. However, bimodality provides the most advantage for air with N_2O < 275 ppbv, where the older peak accounts for a significant fraction of the age spectrum, and for those N_2O levels, there does appear to be a slight trend toward younger mean ages and modal times with increasing altitude.

Midlatitude balloon profiles of CO_2 and SF_6 are typically characterized by a rapid increase in mean age from the tropopause to an altitude between 20 and 25 km with a region of nearly constant mean age of 4-6 years above, extending to the maximum altitude of the profile (~32 km). *Bischof et al.* [1985] proposed that the region with little vertical gradient may result from upwelling of air in the tropics followed by poleward transport at high altitudes. We would add to their interpretation that the rapid increase of mean age in the first few kilometers above the tropopause likely reflects the diminishing contribution of horizontal transport of young air from the tropics over this altitude range. Also, if the only transport process operating in the midlatitude middle stratosphere were downward advection, mean age would decrease with altitude in that region. Since this is not observed, other processes must also be important. For example, limited poleward transport of air across the subtropics could be occurring, but not enough to eliminate the observed ~2 year difference in mean age between the tropics and midlatitudes [*Andrews et al.*, Mean ages of stratospheric air derived from *in situ* observations of CO_2, CH_4 and N_2O, submitted to *J. Geophys. Res.*; *Hall et al.*, 1999; *Neu and Plumb*, 1999] or to fill in the gap between the peaks in the bimodal age spectra. A more detailed model is necessary to explore this question further.

The mean ages and modal times obtained for the older peaks in the bimodal age spectra are considerably older than the transit times along residual circulation pathways calculated by *Rosenlof* [1995], which represent timescales for advection. This difference may be an indicator of the importance of dispersive processes that cause recirculation of air, resulting in longer transit times than expected from advection alone.

Finally, the derived age spectra have implications for interpreting observed differences in tracer relationships between the tropics and midlatitudes. Several recent studies have attempted to quantify the amount of mixing of midlatitude air into the tropical upwelling region using tracer relationships. For example, *Volk et al.* [1996] estimated that at 480 K in the tropics, 40% of the air had come from midlatitudes. Our results provide insight into the extent of recirculation corresponding to this amount of midlatitude air. For example, the midlatitude age spectrum for the 245 ppbv N_2O isopleth (~460 K) is shown in Figure 11 along with the annual mean tropical age spectrum for 460 K found by *Andrews et al.* [1999]. Although the midlatitude air has a mean age of

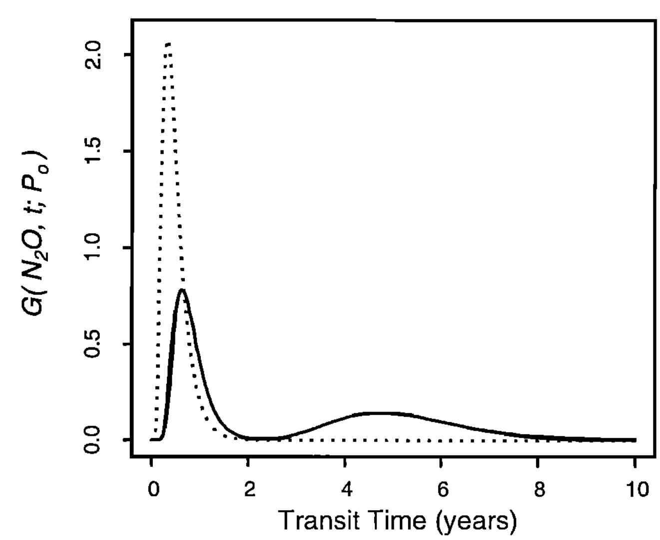

Figure 11. Annual mean tropical age spectrum for 460 K (dotted line) and the midlatitude age spectrum for 245 ppbv N_2O (~460 K, solid line).

2.9 years at this level, ~50% of the air is represented by the younger peak, which has a mean age of only 0.8 year. The annually averaged mean age of the tropical air is ~0.5 year. It is tempting to interpret the difference between the mean age of the tropical air and the mean age of the younger peak in the midlatitude age spectrum, ~0.3 year, as the timescale for mean meridional transport.

Figure 11 suggests that if a significant amount of air enters the tropics by horizontal mixing from midlatitudes, then tropical age spectra could also be bimodal, and the amount of air in the older peak would represent the amount of air being recirculated through the stratosphere. This contingency was not considered by *Andrews et al.* [1999] due to the scarcity of tropical data and a lack of knowledge about the shape of midlatitude age spectra. In principle, we could use the midlatitude age spectra presented here to further address this question, but the limited tropical data are unlikely to adequately constrain proposed bimodal age spectra.

4.3. Comparison of Empirical Age Spectra With 2-D Model Age Spectra

To further explore the significance of our results and to provide a framework for comparing our empirical age spectra with those derived from models, we compared the age spectra derived from CO_2 observations to age spectra generated using the Harvard 2-D model (see, e.g., *Jones et al.* [1998] for a model description) (Figure 12). Note that the objective here is not to evaluate the performance of this particular model, but rather to consider whether bimodal age spectra are physically plausible and to gain some qualitative insight into the mechanisms that contribute to the bimodality. A more detailed analysis of the sensitivity of age spectra and long-lived tracers to assumptions about the rate of overturning in the stratosphere and the permeability of the subtropical barrier using this model is presented in a separate paper [*Jones et al.*, this issue].

The model-generated age spectra clearly contain two peaks, although the peaks are not as distinct as those in the empirical age spectra from CO_2. Bimodality in the model spectra is more apparent at altitudes above (N_2O values below) the range for which empirical age spectra can be derived from CO_2 observations (Figure 12c). (Recall that age spectra can only be derived when both seasonal and long-term trends contribute to the observed CO_2 behavior, and seasonal variations are not detectable for N_2O values less than 235 ppbv.) In general, the model results fall between our bimodal and single-peak cases. In order to compare the observation-based and model results in more detail, fits to the modeled age spectra were obtained using the 1-D bimodal functional form (equation (5)) with a nonlinear least squares fitting routine. The bimodal functional form provided excellent fits to the model spectra, as shown in Figure 12d for the 235 ppbv N_2O level, providing an example of the flexibility of the functional form.

As expected from direct comparison of the spectra, the rms error for the 2-D model falls between the values corresponding to the empirical single-peak and bimodal cases (Figure 4). We used the fits to the model results to compare the area of the younger peak, the mean ages of the individual peaks, and the spectral widths with those for the optimal bimodal solutions found by the genetic algorithm. The fractional area of each peak (Figure 6), the mean ages of each peak and the overall mean age (Figure 7) are quite similar to those for the empirical bimodal spectra. However, both the younger and especially the older peaks are considerably wider in the 2-D model spectra, making the peaks in the 2-D model spectra appear less distinct than the peaks in the optimal bimodal solutions.

Note that the coefficients giving the best fit to the 2-D model age spectra were included in the parameter space searched by the genetic algorithm. Presumably, then if the optimum age spectrum resembled the 2-D model output, it would have been found in our optimization process. To test for an optimum solution in the neighborhood of the 2-D model results, the genetic algorithm was run for the 255 ppbv N_2O surface with an initial population that included the fit to the 2-D model age spectra. The population evolved to give an optimum solution indistinguishable from the original result for that N_2O surface (shown in Figure 3).

In summary, the Harvard 2-D model produces age spectra on N_2O isopleths that are qualitatively and, in several ways, quantitatively similar to the empirical age spectra derived from CO_2 observations, with the major difference being the width of the older peak. This demonstrates that the bimodal-

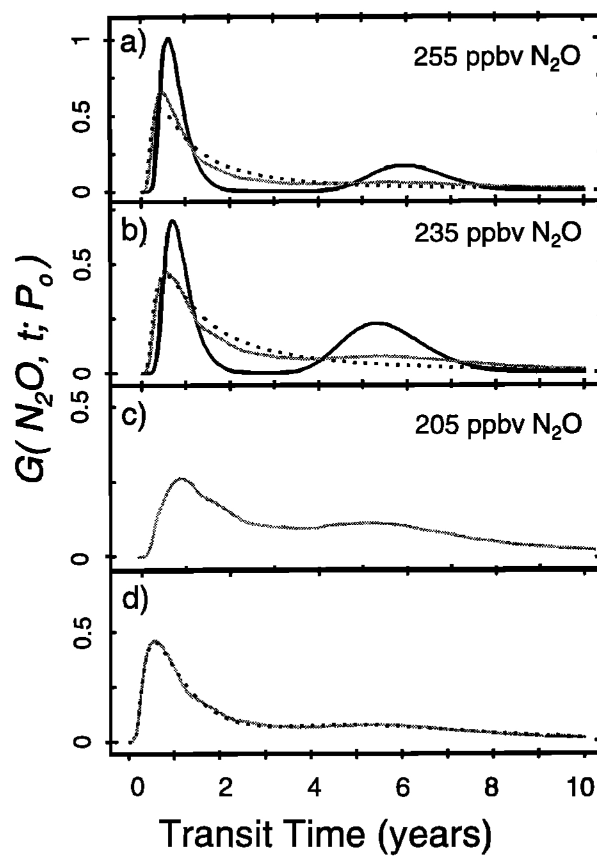

Figure 12. Direct comparison of age spectra for the (a) 255 and (b) 235 ppbv N_2O isopleths from Harvard 2-D model (light solid lines) with the optimum age spectra from the genetic algorithm for the 1-D single peak (dotted lines), the 1-D bimodal (dark solid lines) cases. (c) Results for the 205 ppbv isopleth for the 2-D model. (d) Age spectrum from the Harvard 2-D model for 235 ppbv N_2O (light solid line) shown with the best fit using the 1-D bimodal functional form (dotted line).

ity of the empirical age spectra is consistent with a reasonable parameterization of stratospheric dynamics.

4.4. Uncertainty

In this analysis we have assumed that there is a unique time-independent age spectrum corresponding to each N_2O surface from 235-295 ppbv in the midlatitude lower stratosphere. Before proceeding to other uncertainty issues, such as measurement error and analysis uncertainties, it is important to address whether this is a reasonable assumption, given, for example, path dependent N_2O photochemistry in the stratosphere and its variation with season and latitude.

The photochemical lifetime for N_2O is ~300 years near 20 km, decreasing rapidly with altitude to ~3 years at 30 km and to a few months at 40 km [*Brasseur and Solomon*, 1986]. The extent of photochemical loss of N_2O in an air parcel will therefore depend on the parcel's path through the atmosphere, and air parcels with quite dissimilar transport histories could in principle have the same N_2O value. Thus, the age spectrum on an N_2O isopleth could vary with latitude or with season. We were able to obtain excellent fits to the CO_2 observations without explicitly accounting for seasonal or interannual variation in the age spectrum, presumably because CO_2 and N_2O distributions are affected similarly by temporal variations in transport rates, as discussed above.

With regard to possible latitudinal variation, we note that compact relationships between CO_2 and N_2O are observed in the midlatitude lower stratosphere in essentially all seasons (Figure 2), implying that the timescales for horizontal transport are rapid compared to the lifetimes of both species and to seasonal variations in CO_2 [*Plumb and Ko*, 1992]. It is plausible, then, that if transport rates are sufficiently rapid to produce a constant CO_2 mixing ratio along a given N_2O isopleth, that the age spectrum will be similarly homogenized along isopleths of N_2O. In fact, this appears to be the case in the Harvard 2-D model. Model age spectra are shown in Figure 13 for the 235 ppbv N_2O surface at 32.5°N, 42.5°N, and 52.5°N. *Jones et al.* [this issue] show that the bimodality in the age spectra in that model results from advection of young air from the tropics to latitudes poleward of 32.5° N and downwelling of old air at high latitudes with rapid mixing by eddy diffusion throughout midlatitudes. Clearly, differences in the model age spectra along the isopleth are slight over this latitude range.

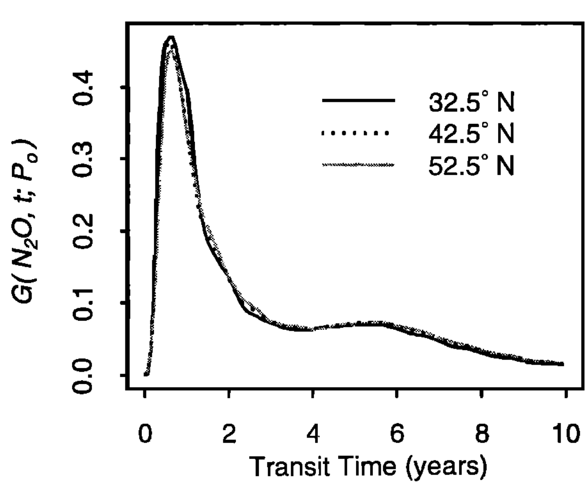

Figure 13. Age spectra from the Harvard 2-D model for three latitudes along the 235 ppbv N_2O isopleth.

One approach for testing for sensitivity to N_2O photochemistry would be to repeat the analysis using tracers with different photochemical lifetimes. For example, the lifetime of CH_4 is ~0.5, 10, and 100 years at 40, 30 and 20 km, while the lifetime of CFC-11 is similar to that for N_2O near 20 km, but just a few days at 40 km [*Brasseur and Solomon*, 1986]. Unfortunately, the long-term precision of the available CH_4 data is not sufficient for this type of analysis, and the use of CFC-11 is complicated by growth in the tropospheric mixing ratio as well as by limitations associated with the sparsity of the measurements. Although the data for the other species are not suitable for defining optimal age spectra, relationships among all potentially available tracers (N_2O [*Podolske and Loewenstein*, 1993], CFC-11 [*Elkins et al.*, 1996], CH_4 [*Elkins et al.*, 1996; *Webster et al.*, 1994], and CFC-12 [*Elkins et al.*, 1996]) were linear and nearly invariant for midlatitude air with N_2O in the range studied here, 295 ppbv $\geq N_2O \geq$ 235 ppbv, from 1992-1998. Thus, we infer that we would obtain similar results if another tracer were used instead of N_2O to define the vertical coordinate.

We next consider uncertainty due to measurement errors in the CO_2 and N_2O data used in this analysis. Frequent in-flight and laboratory calibrations show that the flight-to-flight and year-to-year precision of the CO_2 data is better than 0.1 ppmv throughout the time period considered here. The difference in CO_2 rms error between the optimal bimodal and single-peaked age spectra ranges from 0.09 to 0.16 ppmv for N_2O values from 235 to 295 ppbv, with the largest difference for N_2O = 255 ppbv. Although these differences approach the limits of instrument precision, Figure 3 shows that the bimodal spectra produce simulated CO_2 time series that more accurately capture the temporal variations in CO_2 on an isopleth, particularly for air with N_2O < 275 ppbv where the area of the older peak is relatively large.

Significant improvements were made to the ATLAS instrument after the SPADE mission (1992-1993), and the measurement errors for N_2O during SPADE were 7% compared to 3.5% during subsequent deployments [*Strahan et al.*, 1999]. Careful inspection of Figure 3 shows that the SPADE data contribute significantly to the difference in CO_2 rms error between the single-peaked and bimodal age spectra. When the SPADE data were excluded from the optimization, the rms error for the single-peaked case improved substantially while that for the bimodal case was largely unaffected, so that the difference in fitness decreased from a factor of 1.8 to a factor of 1.25. The improvement in the single-peaked case occurred because, with a shorter record, the constraint imposed by interannual variability in the CO_2 growth rate was relaxed. However, the shapes of the derived age spectra were not significantly affected by excluding the SPADE data, and the time series generated by the bimodal spectra fit the SPADE data well, even though they were not included in the optimization. Furthermore, part of the increased uncertainty in the N_2O measurements during SPADE was due to a problem with correcting for changes in temperature and pressure when the plane was rapidly changing altitude. The bimodal age spectra provide the most advantage for altitudes corresponding to N_2O < 275 ppbv, since at lower altitudes (higher N_2O) the contribution of the second peak to the total area of the age spectrum is relatively small, and these data were primarily obtained during level flight.

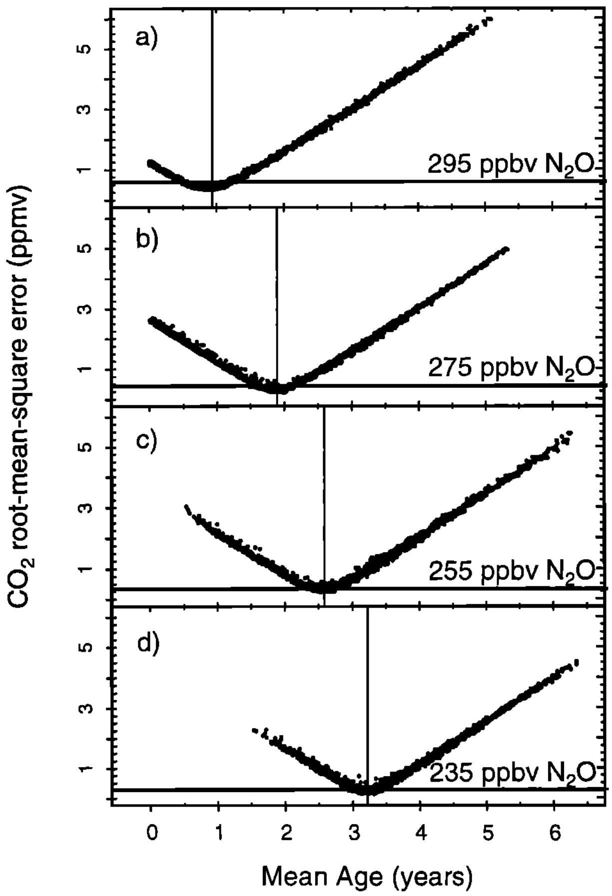

Figure 14. Variation of CO_2 root-mean-square error with mean age for near-optimum solutions (1-D bimodal case) for several isopleths of N_2O. Dashed horizontal lines represent an increase of a factor of 1.5 in the rms error of the optimum solution. Vertical lines represent the optimum mean age.

Finally, we consider the sensitivity of our fitness criterion, the CO_2 rms error, to the parameters of the derived age spectra. According to equation (5), the bimodal age spectrum is completely specified by five parameters, A_1, B_1, B_2, C_1, and C_2. Equivalently, the age spectrum can be described in terms of the mean ages and modal times of each peak and the overall mean age (or the relative area of the peaks).

The relationship between overall mean age and N_2O shown in Figure 7b is an especially robust result of the current study. We used a Monte Carlo approach to quantify the sensitivity of derived mean ages to uncertainties in parameters for the age spectra. For each N_2O surface, 5000 candidate solutions were generated by applying randomly generated perturbations of up to $\pm 50\%$ to the five parameters (the mean age and modal time of each peak and the relative area) describing the optimum bimodal solution. The resulting relationship between overall mean age and CO_2 rms error is shown for several N_2O isopleths in Figure 14. Mean age appears to be a primary predictor of rms error, at least for the near optimum solutions. Note, however, that it is possible to generate age spectra with a near optimum mean age that have much higher rms error than the optimum solution. For example, for 295 ppbv N_2O, a single peaked age spectrum with a mean age of 0.93 year and a modal time of 0.88 year has an rms error of 1.2 ppmv, while for the optimum solution it is 0.37 ppmv.

We performed a separate analysis of the sensitivity of the CO_2 rms error to the mean ages and modal times of the individual peaks. The mean age and modal time of one peak were held constant while the mean age and modal time for the other peak were varied about their optimal solutions. The overall mean age was held constant by adjusting the relative areas of the two peaks. Results are shown in Figure 15, where contours of the CO_2 rms error are indicated as a function of mean age and modal time for each N_2O level. For all N_2O levels the modal time for the younger peak is better constrained than the mean age of that peak. Not surprisingly, the mean age and modal time of the older peak are more tightly constrained for 255 and 235 ppbv N_2O than for higher N_2O mixing ratios, because the relative area of the older peak increases with decreasing N_2O.

In order to interpret the results shown in Figures 14 and 15, we must determine what differences in the CO_2 rms error are significant. One possible benchmark is the average over the 15 deployments of the standard deviation of the observed CO_2 mixing ratios for each N_2O level, which varies from to 0.16 ppmv at 235 ppbv N_2O to 0.28 ppmv at 295 ppbv N_2O. For comparison the rms error corresponding to the optimal solutions ranges from 0.15 ppmv at 235 ppbv N_2O to 0.37 ppmv at 295 ppbv N_2O. Thus, adopting the average standard deviation of the data as the standard for defining uncertainty (i.e., only differences in CO_2 rms error larger than the average standard deviation for the N_2O level would be considered significant) would be roughly equivalent to doubling the optimum rms error. However, visual inspection of Figure 3 suggests that this standard allows an excessive range of near optimum solutions. For example, consider the optimum age spectra for 235 ppbv N_2O. The CO_2 rms error for the single-peaked spectrum is 0.15 ppmv higher than that for the bimodal case (i.e., a factor of 2 higher), but the fit to the observations is clearly much better for the bimodal case, indicating that the genetic algorithm is able to discriminate among possible solutions based on differences in the CO_2 rms error that are smaller than the average standard deviation of the observations. This should not be surprising, since random instrument noise contributes variance for both CO_2 and N_2O, but this noise averages out in the huge data set used in this analysis. For the purposes of assigning uncertainty to our estimates of the overall mean age, we used the range of mean ages in solutions with an rms error within a factor of 1.5 of that for the optimum solution. This criterion corresponds to rms errors within 0.2 ppmv of the optimum for 295 ppbv N_2O and within 0.08 ppmv of the optimum for 235 ppbv N_2O and to uncertainty in the mean age of 0.3 year for 295 ppbv N_2O and 0.1 year for 235 ppbv N_2O.

To summarize, comparison of Figures 14 and 15 shows that the CO_2 rms error is more sensitive to changes in the overall mean age of the spectrum than to the details of the shape. Note, however, that these uncertainty analyses, like the optimizations, were carried out as if the CO_2 time series on neighboring N_2O surfaces were independent, which they most certainly are not. The fact that we obtained relatively smooth and monotonic profiles of mean age and modal time for both peaks is unlikely to be fortuitous, nor is the similarity between the range of transit times encompassed by the older peak and mean ages observed in the midlatitude middle stratosphere. We have shown that these results are not sensitive to the functional form by repeating the analysis using the

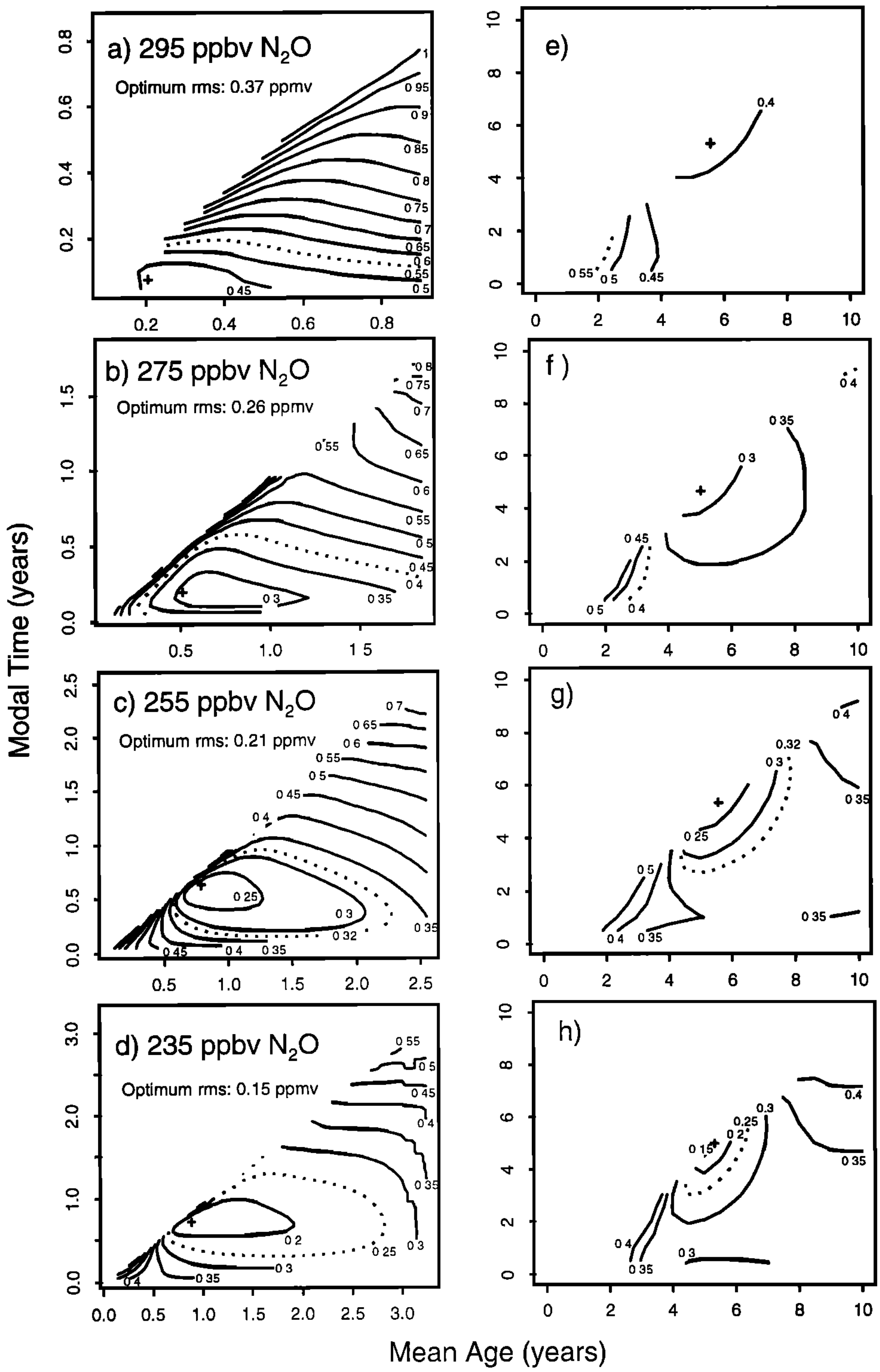

Figure 15. (a-d) Sensitivity of results to variation in the mean age and modal time of the younger peak with the overall mean age and the mean age and modal time of the second peak held constant. Pluses indicate optimum solutions. Contours are values of CO_2 rms error. (e-h) Same as Figures 15a-15d, but for the older peak. Dashed contours correspond to an increase of a factor 1.5 in the optimum rms error.

bimodal boxcar function. Furthermore, we searched for a solution in the neighborhood of the 2-D model spectra and recovered our original results, and we were unable to improve the fit to the CO_2 observations by using functions comprised of three peaks. Thus we believe that our bimodal age spectra reflect fundamental timescales for the stratospheric circulation.

5. Conclusions

We have shown that age spectra for the lower midlatitude stratosphere can be derived from a set of high-quality observations of CO_2 and N_2O. Our method provides a robust relationship between mean age and N_2O for mean ages up to ~3.25 years, independent of season. We have described a detailed framework for comparing our results with those from models that does not require an accurate representation of the CO_2 boundary condition and is independent of the details of dates and locations of the available CO_2 measurements, and we have presented the first observations of the propagation of interannual variations in the CO_2 growth rate into the stratosphere.

The derived age spectra provide new quantitative insight into transport processes throughout the stratosphere, while presenting an overall picture that is consistent with the current understanding of the general circulation. The clear separation of the two peaks in the derived age spectra is consistent with a circulation characterized by two predominant routes by which air enters the midlatitude lower stratosphere. We argue that the younger peak results from rapid quasihorizontal transport from the tropics, due to both mean motions and to eddies, while the older peak represents downwelling of air from higher altitudes in the mean meridional circulation. Our results suggest that the mean age of air in the midlatitude lower stratosphere is determined by the relative importance of these two pathways, rather than by a small amount of very old air in the tail of the age spectrum. Finally, the mean age of the older peak is similar to mean ages observed at higher altitudes in the midlatitude stratosphere, as expected if that region is the source of the air represented by the older peak.

Appendix A: Details of the Genetic Algorithm

A detailed description of genetic algorithms is given by *Beasely et al.* [1993a, 1993b, and references therein]. The method was first fully documented by *Holland* [1975]. Briefly, a candidate solution is represented as a string of binary numbers, which are called "chromosomes," where each binary digit represents one gene. The length of the chromosome is determined by the range of solutions and the required resolution, below which solutions are effectively identical. An initial population of solutions is created using a random number generator. The "fitness" of each individual solution is determined, and those individuals with higher fitness are assigned a greater probability of reproducing. A mating pool is selected, and individuals are randomly grouped into mating pairs. Two offspring are created from each mating pair by swapping a randomly selected segment of the parents' chromosomes. The offspring are then subjected to random mutations with a chosen (usually low) probability. The average fitness of the new generation will be higher than the previous, and the process is repeated until the population converges or for a specified number of generations.

For our problem, each solution is a set of three or five parameter values describing the age spectrum for a particular N_2O value. We used 15 genes per coefficient (for a total of 75 genes per chromosome for the bimodal cases) and a population size of 50. For each candidate solution, we calculated the CO_2 mixing ratios corresponding to the date of the observations for each deployment for which we have NH midlatitude data. The fitness criterion was the root-mean-square (rms) difference between the predicted CO_2 mixing ratios and the observations:

$$CO_2\ \mathrm{rms} = \sqrt{\frac{\sum (CO_2^{\,OBS} - CO_2^{\,PRED})^2}{N_{OBS}}}. \qquad \text{(A1)}$$

The most challenging aspect of implementing a genetic algorithm is defining a relationship between the fitness criterion and likelihood of reproduction. This relationship is known as the "fitness function" and may be based on the absolute value of the fitness criterion (e.g., a solution with an rms error of 0.1 ppm may be assigned a 90% probability of reproduction while one with an rms error of 1 ppm may have a probability of 10%) or on the relative fitness within a generation (e.g., the top 10% of the population may be assigned a 90% chance of reproducing while the bottom 10% are given only a 1% chance). The selection of an appropriate fitness function is critical for the success of the optimization. If the fitness function is too "steep," so that only the best solutions have a significant chance of reproducing, the population may converge prematurely on a local optimum. Conversely, if the fitness function is not steep enough, the optimization will be inefficient or the solution may be elusive.

We obtained the best results using "tournament matching" to define reproductive success. In this method, pairs or groups of individuals are selected randomly (with replacement), and the individual with the lowest rms error is placed in the mating pool. This process is repeated until the mating pool has the same size as the initial population. The steepness of the fitness function is determined by the tournament size. We obtained the best results using a tournament size of 2. We also placed a randomly generated solution into the mating pool in an effort to prevent the genetic algorithm from converging on a local minimum. The individuals were then grouped into mating pairs, each of which produced two offspring.

The two stages of the mating process are "crossover" and "mutation." During crossover, a randomly chosen segment of the parents' chromosomes are swapped. We chose a different segment for each mating pair. Typically, a small percentage of the pairs skip the crossover stage. After crossover the offspring are subjected to random mutations where 1s are changed to 0s and vice versa. We used a probability of crossover of 0.8-0.9 and a probability of mutation 0.025. Finally, we replaced one member of the new population with a clone of the most fit individual from the previous generation. This significantly improved the performance of the optimization.

We performed 3-5 optimizations with different starting populations for each of the three functional forms on each N_2O isopleth, with 5000 generations per optimization.

We performed several tests to evaluate the reliability of the genetic algorithm used in this analysis. For example, synthetic CO_2 data were generated with the same temporal resolution as the ER-2 data using a variety of randomly selected single-mode and bimodal age spectra, and we then attempted to recover the age spectrum used to generate the data. We found that the algorithm using the 1-D bimodal functional form performed better when set to search for optimal mean ages and modal times for each peak instead of searching for the coefficients B_1, B_2, C_1, and C_2 directly. This transformation effectively shrinks the solution space by reducing the nonlinearity of the problem, and thereby increases the efficiency of the algorithm. We determined that the bimodal algorithm, constrained by data generated with a single-mode spectrum, reliably recovered the original single-mode spectrum, demonstrating that the bimodality we found in the analysis of atmospheric data is not an artifact of the algorithm.

Acknowledgments. We thank C. R. Webster and coworkers for providing CH_4 data; T. P. Bui and coworkers for measurements of potential temperature and latitude; T J. Conway for providing surface station data for CO_2; and T. M. Hall and M. R. Schoeberl for suggestions on how to address uncertainty associated with using N_2O as the vertical coordinate for this analysis. We are grateful for the efforts of all the ER-2 investigators, coordinators, pilots, and crew. This research was supported by NASA's Upper Atmospheric Research Program and Atmospheric Effects of Aviation Project/ High Speed Research Program.

References

Andrews, A. E., K. A. Boering, B C. Daube, S. C. Wofsy, E. J. Hintsa, E. M Weinstock, and T. P. Bui, Empirical age spectra for the lower tropical stratosphere from in situ observations of CO_2. Implications for stratospheric transport *J. Geophys. Res*, *104*, 26,581-26,595, 1999.

Avallone, L. M., and M. J. Prather, Photochemical evolution of ozone in the lower tropical stratosphere, *J. Geophys Res*, *101*, 1457-1461, 1996

Bacmeister, J. T., D E. Siskind, M. E. Summers, and S. D Eckerman, Age of air in a zonally averaged two-dimensional model, *J Geophys. Res*, *103*, 11,263-11,288, 1998.

Beasely, D, D R. Bull, and R. R. Martin. An overview of genetic algorithms,1, Fundamentals, *Univ. Comput.*, *15*, 58-69, 1993a.

Beasely, D., D. R. Bull, and R. R. Martin, An overview of genetic algorithms, 2, Research topics, *Univ. Comput.*, *15*, 170-181, 1993b.

Bischof, W., P. Fabian, and R. Borchers, Decrease in CO_2 mixing ratio observed in the stratosphere, *Nature*, *288*, 347-348, 1980

Bischof, W, R Borchers, P. Fabian, and B. C. Kruger, Increased concentration and vertical distribution of carbon dioxide in the stratosphere, *Nature*, *316*, 708-710, 1985

Boering, K. A., B C Daube, S C Wofsy, M. Loewenstein, J. R. Podolske, and E R. Keim, Tracer-tracer relationships and lower stratospheric dynamics: CO_2 and N_2O correlations during SPADE, *Geophys Res. Lett*, *21*, 2567-2570, 1994

Boering, K A., et al, Measurements of stratospheric carbon dioxide and water vapor at northern midlatitudes· Implications for troposphere-to-stratosphere transport, *Geophys. Res. Lett*, *22*, 2737-2740, 1995.

Boering, K A., S C Wofsy, B C. Daube, H. R. Schneider, M Loewenstein, J. R. Podolske, and T. J Conway, Stratospheric mean ages and transport rates from observations of carbon dioxide and nitrous oxide, *Science*, *274*, 1340-1343, 1996.

Brasseur, G, and S. Solomon, *Aeronomy of the Middle Atmosphere*, 2nd ed., 452 pp., D Reidel, Norwell, Mass., 1986.

Chen, P., J. R. Holton, A. O'Neill, and R. Swinbank, Isentropic mass exchange between the tropics and extratropics in the stratosphere, *J. Atmos. Sci.*, *51*, 3006-3018, 1994.

Conway, A. J., and P. A. Bland, A genetic algorithm for pairing meteorite finds, *Meteorit Planet. Sci.*, *33*, 491-499, 1998.

Conway, T. J., P. P Tans, L. S. Waterman, K. W. Thoning, D. R. Kitzis, K. A. Masarie, and N Zhang, Evidence for interannual variability of the carbon cycle from the National Oceanic and Atmospheric Administration/ Climate Monitoring and Diagnostics Laboratory global air sampling network, *J. Geophys. Res.*, *99*, 22,831-22,855, 1994

Deshler, T., B. J. Johnson, and W. R. Rozier, Balloonborne measurements of Pinatubo aerosol during 1991 and 1992 at 41° N: Vertical profiles, size distribution, and volatility, *Geophys. Res. Lett.*, *20*, 1435-1438, 1993

Ehhalt, H. D., P. E. Roth, and U. Schmidt, On the temporal variation of stratospheric trace gas concentrations, *J. Atmos. Chem.*, *1*, 27-51, 1983.

Elkins, J. W., et al., Airborne gas chromatograph for in situ measurements of long-lived species in the upper troposphere and lower stratosphere, *Geophys. Res. Lett.*, *23*, 347-350, 1996.

Feely, H. M., and J. Spar, Tungsten-185 from nuclear bomb tests as a tracer for stratospheric meteorology, *Nature*, *188*, 1062-1088, 1960.

Fleming, E. L., C H. Jackman, R. S. Stolarski, and D B. Considine, Simulation of stratospheric tracers using an improved empirically based model transport formulation, *J. Geophys. Res*, *104*, 23,911-23,934, 1999

Flocke, F., et al., An examination of chemistry and transport processes in the tropical lower stratosphere using observations of long-lived and short-lived compounds obtained during STRAT and POLARIS, *J. Geophys. Res.*, *104*, 26,625-26,642, 1999.

Goldan, P. D., W. C. Kuster, D. L. Albritton, and A. L. Schmeltkopf, Stratospheric $CFCl_3$, CF_2Cl_2, and N_2O height profile measurements at several altitudes, *J. Geophys. Res.*, *85*, 413-423, 1980.

Grant, W. B., E. V. Browell, C. S. Long, L. L. Stowe, R. G. Grainger, and A Lambert, Use of volcanic aerosols to study the tropical stratospheric resevoir, *J. Geophys. Res.*, *101*, 3973-3988, 1996.

Hall, T. M., and R. A. Plumb, Age as a diagnostic of stratospheric transport, *J. Geophys. Res.*, *99*, 1059-1070, 1994.

Hall, T. M., and M. J. Prather, Simulations of the trend and annual cycle in stratospheric CO_2, *J. Geophys. Res.*, *98*, 10,573-10,581, 1993

Hall, T M., and D W Waugh, Timescales for the stratospheric circulation derived from tracers, *J Geophys Res.*, *102*, 8991-9001, 1997.

Hall, T M., and D W Waugh, Stratospheric residence time and its relationship to mean age, *J Geophys Res*, *105*, 6773-6782, 2000.

Hall, T. M, D. W. Waugh, K. A. Boering, and R. A Plumb, Evaluation of transport in stratospheric models, *J. Geophys Res.*, *104*, 18,815-18,839, 1999.

Harnisch, J, R Borchers, P. Fabian, and M. Maiss, Tropospheric trends for CF_4, and C_2F_6 since 1982 derived from SF_6 dated stratospheric air, *Geophys. Res. Lett.*, *23*, 1099-1102, 1996.

Harnisch, J., W. Bischof, R Borchers, P. Fabian, and M Maiss, A stratospheric excess CO_2 - due to tropical deep convection, *Geophys. Res. Lett*, *25*, 63-66, 1998.

Herman, R. L., et al, Tropical entrainment timescales inferred from stratospheric N_2O and CH_4 observations, *Geophys. Res. Lett.*, *25*, 2781-2784, 1998

Hintsa, E J., E. M. Weinstock, A. E Dessler, J. G. Anderson, M. Loewenstein, and J. R. Podolske, SPADE H_2O measurements and the seasonal cycle of stratospheric water vapor, *Geophys Res. Lett*, *21*, 2559-2562, 1994

Holland, J H, Adaptation in Natural and Artificial Systems, Univ. Mich Press, Ann Arbor, 1975.

Holton, J. R, P H. Haynes, M. E. McIntyre, A. R. Douglass, R. B. Rood, and L. Pfister, Stratosphere-troposphere exchange, *Rev. Geophys*, *33*, 405-439, 1995.

Johnson, D. G, K. W Jucks, W. A. Traub, and K. V. Chance, G. C. Toon, J M Russel, and M. P McCormick, Stratospheric age spectra derived from observations of water vapor and methane, *J Geophys Res.*, *104*, 21,595-21,602, 1999.

Jones, D. B. A., H. R Schneider, and M. B McElroy, Effects of the quasi-biennial oscillation on the zonally averaged transport of tracers, *J Geophys. Res.*, *103*, 11,235-11,249, 1998.

Jones, D. B. A., A. E. Andrews, H R Schneider, and M. B. McElroy, Constraints on meridional transport in the stratosphere imposed by the mean age of air in the lower stratosphere, *J. Geophys. Res.*, this issue

Kawa, S. R., et al., Assessment of the effects of high-speed aircraft in the stratosphere: 1998, *NASA Tech. Publ.*, *NASA/TP-99-209236*, 1999.

Keeling, C. D., and T. P. Whorf, Atmospheric CO_2 records from sites in the SIO air sampling network, in *Trends '93: A Compendium of Data on Global Change*, *Rep. ORNL/CDIAC-65*, edited by T. A. Boden et al., pp. 16-26, Carbon Dioxide Inf. Anal. Cent., Oak Ridge Nat. Lab., Oak Ridge, Tenn., 1994

Keeling, C. D., T. P. Whorf, M. Wahlen, and J van der Plicht, Interannual extremes in the rate of rise atmospheric carbon dioxide since 1980, *Nature*, *375*, 666-670, 1995.

Kida, H., General circulation of air parcels and transport characteristics derived from a hemispheric GCM, 2, Very long term motions in the troposphere and stratosphere, *J. Meteorol. Soc. Jpn.*, *61*, 510-522, 1983.

King, S. D., Radial models of mantle viscosity: Results from a genetic algorithm, *Geophys. J. Int.*, *122*, 725-734, 1995.

Kinnison, D. E., H. S Johnston, and D. J. Wuebbles, Model study of atmospheric transport using carbon-14 and strontium-90 as inert tracers, *J. Geophys. Res.*, *99*, 20,647 - 20,664, 1994.

Li, S, and D W. Waugh, Sensitivity of mean age and long-lived tracers to transport parameters in a two-dimensional model, *J.*

Geophys. Res., *104*, 30,559-30,569, 1999.
Maiss, M., L. P. Steele, R. J. Francey, P J. Fraser, R. L Langenfelds, N. B A Trivett, and I. Levin, Sulfur hexafluoride: A powerful new atmospheric tracer, *Atmos. Environ*, *30*, 1621-1629, 1996.
McCormick, M. P., and R. E. Veiga, SAGE II measurements of early Pinatubo Aerosols, *Geophys. Res. Lett.*, *19*, 155-158, 1992.
Michelsen, H. A., G L. Manney, M. R. Gunson, and R Zander, Correlations of stratospheric abundances of NO_y, O_3, N_2O, and CH_4 derived from ATMOS measurements, *J. Geophys. Res.*, *103*, 28,347-28,359, 1998.
Minschwaner, K., A E. Dessler, J. W. Elkins, C. M. Volk, D W. Fahey, M. Loewenstein, J. R Podolske, A. E. Roche, and K. R. Chan, The bulk properties of isentropic mixing into the tropics in the lower stratosphere, *J. Geophys. Res.*, *101*, 9433-9439, 1996.
Mote, P. W., T. J. Dunkerton, M. E. McIntyre, E. A. Ray, P. H. Haynes, and J. M Russell III, Vertical velocity, vertical diffusion, and dilution by midlatitude air in the tropical lower stratosphere, *J. Geophys. Res.*, *103*, 8651-8666, 1998.
Murphy, D. M., et al., Reactive nitrogen and its correlation with ozone in the lower stratosphere and upper troposphere, *J. Geophys. Res.*, *98*, 8751-8773, 1993
Nash, E. R., P. A. Newman, J. E. Rosenfield, and M. R. Schoeberl, An objective determination of the polar vortex using Ertel's potential vorticity, *J. Geophys. Res.*, *101*, 9471-9478, 1996.
Neu, J. L., and R. A. Plumb, The age of air in a "leaky pipe" model of strospheric transport, *J. Geophys. Res.*, *104*, 19,243-19,255, 1999
Park, J. H., M. K. W Ko, C. H. Jackman, J. A. Kaye and K H. Sage (Eds.), Models and measurements intercomparison II, *NASA Tech. Memo., NASA/TM-1999-209554*, 1999
Plumb, R. A., A "tropical pipe" model of stratospheric transport, *J. Geophys. Res*, *101*, 3957-3972, 1996.
Plumb, R. A., and M. K. W Ko, Interrelationships between mixing ratios of long-lived stratospheric constitutents, *J. Geophys. Res*, *97*, 10,145-10,156, 1992.
Podolske, J. R, and M Loewenstein, Airborne tunable diode laser spectrometer for trace-gas measurement in the lower stratosphere, *Appl. Opt.*, *32*, 5324-5333, 1993
Randel, W. J, J C Gille, A E. Roche, J. B. Kumer, J L. Mergenthaler, J W Waters, E. F Fishbein, and W. A. Lahoz, Stratospheric transport from the tropics to middle latitudes by planetary-wave mixing, *Nature*, *365*, 533-535, 1993.
Ray, E. A., et al., Transport into the Northern Hemisphere lowermost stratosphere revealed by in situ tracer measurements, *J. Geophys. Res.*, *104*, 26,565-26,580, 1999.
Rosenlof, K. H., Seasonal cycle of the residual mean circulation in the stratosphere, *J. Geophys. Res.*, *100*, 5173-5191, 1995.
Schmidt, U., and A. Khedim, In situ measurements of carbon dioxide in the winter Arctic vortex and at midlatitudes: An indicator of the "age" of stratospheric air, *Geophys. Res. Lett.*, *18*, 763-766, 1991.
Schoeberl, M. R., L. C Sparling, C. H. Jackman, and E. L. Fleming, A Lagrangian view of stratospheric trace gas distributions, *J. Geophys. Res.*, *105*, 1537-1552, 2000.
Scott, S. G., T. P. Bui, K R. Chan, and S W. Bowen, The meteorological measurements system on the NASA ER-2 aircraft, *J Atmos. Oceanic Technol.*, *7*, 525-540, 1990.
Strahan, S E., A. R. Douglass, J. E Nielsen, and K. A. Boering, The CO_2 seasonal cycle as a tracer of transport, *J. Geophys Res.*, *103*, 13,729-13,741, 1998
Strahan, S. E., M. Loewenstein, and J. R. Podolske, Climatology and small-scale structure of lower stratospheric N_2O based on in situ observations, *J. Geophys. Res*, *104*, 2195-2208, 1999
Strunk, M., et al., CO_2 and SF_6 as stratospheric age tracers: Consistency and the effect of mesospheric SF_6 loss, *Geophys. Res. Lett.*, *27*, 341-344, 2000.
Telegadas, K., and R. J. List, Are particulate radioactive tracers indicative of stratospheric motions?, *J. Geophys. Res.*, *74*, 1339-1350, 1969.
Trepte, C. R., and M. H. Hitchman, Tropical stratospheric circulation deduced from satellite aerosol data, *Nature*, *355*, 626-628, 1992
Trepte, C. R., R. E. Veiga, and M. P. McCormick, The poleward dispersal of Mount Pinatubo volcanic aerosol, *J. Geophys. Res*, *98*, 18,563-18,573, 1993.
U. S. Department of Commerce, Summary Report 1994-95, *Clim. Monit. Diagnostics Lab. Rep. 23*, edited by D. J. Hofmann, Washington, D. C. 1996.
Volk, C. M., et al., Quantifying transport between the tropical and mid-latitude lower stratosphere, *Science*, *272*, 1763-1768, 1996.
Volk, C M., et al., Evaluation of source gas lifetimes from stratospheric observations, *J. Geophys. Res.*, *102*, 25,543-25,564, 1997
Waugh, D. W., Seasonal variation of isentropic transport out of the tropical stratosphere, *J. Geophys. Res*, *101*, 4007-4023, 1996.
Webster, C. R., R. D. May, C. A. Trimble, R. G. Chave, and J. Kendall, Aircraft (ER-2) laser infrared absorption spectrometer (ALIAS) for in situ stratospheric measurements of HCl, N_2O, CH_4, NO_2, and HNO_3, *Appl. Opt.*, *33*, 454-472, 1994.

A. E Andrews, NASA Goddard Space Flight Center, Mailstop 916.0, Greenbelt, MD 20771 (andrews@code916 gsfc.nasa.gov).
S. Alex, B. C. Daube, D. B. Jones, and S C. Wofsy, Department of Earth and Planetary Sciences and the Division of Engineering and Applied Sciences, 20 Oxford St., Harvard University, Cambridge, MA 02138
K. A. Boering, Departments of Chemistry and of Earth and Planetary Science, University of California, Berkeley, CA 94720
M. Loewenstein and J. R. Podolske, NASA Ames Research Center, Mailstop 245-5, Moffett Field, CA 94035.
S. E. Strahan, NASA Goddard Space Flight Center, Mailstop 910.3, Greenbelt, MD 20771

(Received July 18, 2000; accepted October 31, 2000.)